13

Interior Composition, Structure and Dynamics of the Galilean Satellites

G. Schubert
University of California, Los Angeles

J. D. Anderson
Jet Propulsion Laboratory, California Institute of Technology

T. Spohn
Westfälische Wilhelms-Universität Münster

W. B. McKinnon
Washington University, St. Louis

13.1 INTRODUCTION

In this chapter we discuss the structure, composition, and dynamical states of the interiors of Io, Europa, Ganymede, and Callisto. Interior structure and composition models of the Galilean satellites are constrained by gravity and magnetic field data and information from imaging and infrared observations. Because gravity data provide the principal constraints, we begin with a detailed discussion of them. Other relevant data are referred to in the discussions that follow of each of the satellites. The reader can find additional information about the magnetic, imaging, and infrared observations in other chapters of this book.

The interior models developed in this chapter are sketched in Figure 13.1. Metal, rock, and water are the main constituents of the interiors, though Io has no water. Rock and metal have separated inside Io to form a metallic core and silicate mantle. A similar differentiation has occurred in Europa and Ganymede, which also have water ice–liquid shells surrounding their rocky mantles. Interestingly, if the water shells could be removed from Europa and Ganymede, all three inner Galilean satellites would be very much alike in terms of overall size and internal structure. Only Callisto stands apart; it has no metallic core, and rock (plus metal) and ice are still intimately mixed throughout much if not all of the deep interior. We now proceed to elaborate on the basis for these models and what they imply for the origin and evolution of the satellites.

13.2 GRAVITATIONAL FIELDS OF THE SATELLITES

Detection of the subtle deflection of a spacecraft's trajectory as it passes close to a planetary body is a valuable tool for measuring the object's gravitational field. Doppler data generated by stations of the Deep Space Network (DSN), using the *Galileo* spacecraft's radio communication system at S band (2.3 GHz), have been used to determine the mass and gravitational quadrupole moments of the four Galilean satellites. The resulting triaxial fields are consistent with the assumption that the satellites are in tidal and rotational equilibrium. Accordingly, interior models can be constructed which are consistent with two reduced data, the mean density determined from the satellite's mass and radius, and the axial moment of inertia determined from the quadrupole moments. With such limited data it is useful to examine simple three-layer models of the satellites. In such models, which can be easily reduced to two zones, the mean density $\bar{\rho}$ is given in terms of a core density ρ_c, a mantle density ρ_m and a shell density ρ_s by

$$\bar{\rho} = \rho_s + (\rho_c - \rho_m)\left(\frac{r_c}{R}\right)^3 + (\rho_m - \rho_s)\left(\frac{r_m}{R}\right)^3 \qquad (13.1)$$

where r_c is the core radius, r_m is the mantle radius, and R is the mean surface radius.

This density constraint can be obtained from flybys that are not necessarily close. For example, the *Pioneer* and *Voyager* spacecraft provided GM values (G is the gravitational constant and M is the total satellite mass) for all four satellites (Campbell and Synnott 1985). However, even in two-layer models where $\rho_m = \rho_s$, there is only one equation in three unknowns (ρ_c, ρ_s, r_c). More data are needed, and they are provided by the *Galileo* spacecraft's close flybys. From a sufficiently far distance, the gravitational field of any body can be represented by a point mass. When the body is approached at a closer distance, and with the origin of coordinates taken at the center of mass, the quadrupole moments are the first higher-degree moments that can be detected. In fact, for any arbitrary mass distribution, MacCullagh's formula (Danby 1988), which includes GM and the quadrupole moments, can be used to approximate the gravi-

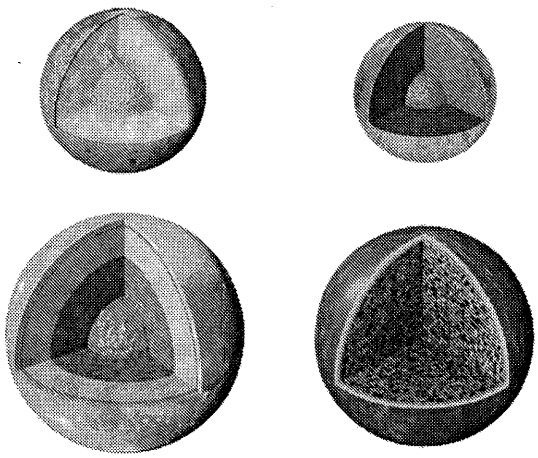

Figure 13.1. Model interiors of the Galilean satellites. Io is at the top left, Europa is at the top right, Ganymede is at the bottom left, and Callisto is at the bottom right. The surfaces of the satellites are mosaics of images obtained from NASA's *Voyager* and *Galileo* spacecrafts, and the interior characteristics are inferred from gravity field and magnetic field measurements by the *Galileo* spacecraft. The satellites are shown according to their actual relative sizes. Io, Europa, and Ganymede have metallic (iron, nickel) cores (shown in gray) of unknown composition and radius surrounded by rocky mantles. Europa and Ganymede have water shells that are mostly ice but which partially contain liquid water oceans of unknown thickness at uncertain depth. Callisto's deep interior is a mixture of rock (and metal) and ice surrounded by a shell of relatively clean ice that probably has an internal liquid water ocean. Callisto could also have a relatively thin ice skin that contains a substantial rock component as well as a small rock core. This revised figure, based on the JPL release PIA01082, was prepared with the help of Zareh Gorjian and Eric M. DeJong (JPL), Pam Engebretson, and Robert Pappalardo (University of Colorado).

tational potential. Alternatively, we use a truncated form of the standard Legendre expansion of the potential function V in spherical harmonics (Kaula 1966),

$$V(r,\phi,\lambda) = \frac{GM}{r}[1+\sum_{n=2}^{\infty}\sum_{m=0}^{n}\left(\frac{R}{r}\right)^n (C_{nm}\cos m\lambda + S_{nm}\sin m\lambda)P_{nm}(\sin\phi)] \quad (13.2)$$

The spherical coordinates (r, ϕ, λ) are referred to the center of mass, with r the radial distance, ϕ the latitude, and λ the longitude on the equator. P_{nm} is the associated Legendre polynomial of degree n and order m, and C_{nm} and S_{nm} are the corresponding harmonic coefficients.

The Galilean satellites are synchronously rotating with their orbital periods.* Hence, for purposes of the *Galileo* flybys, they are in static equilibrium with relatively large deformations caused by rotational and tidal forcing, so we restrict analysis to interior models consistent with equilibrium theory (Kaula 1968, Hubbard and Anderson 1978, Rappaport *et al.* 1997). The smaller dynamical tidal perturbations caused by the orbital eccentricity e are unobservable with the *Galileo* spacecraft, even for Europa, which has the largest forced eccentricity ($e = 0.0101$) of the four satellites (Greenberg 1982). The only nonzero gravity parameters of importance are therefore the monopole GM, and the two quadrupole coefficients J_2 ($-C_{20}$) (the dynamical polar flattening) and C_{22} (the dynamical equatorial flattening). These coefficients, along with other parameters in the fitting model, are determined from the *Galileo* radio Doppler data by weighted least squares (Tapley 1973, Anderson 1974, Lawson and Hanson 1974, Moyer 2000).

In principle, given enough flybys, or an orbiter, the gravity coefficients J_2 and C_{22} can be inferred from the Doppler data as two separate independent parameters. However, in practice, for only two or at most a few close flybys, J_2 and C_{22} are not independent. The measure of independence is given by the statistical correlation coefficient μ, which is zero for complete independence and unity for complete dependence. When the correlation is nearly unity, as in the case of Europa, Ganymede, and Callisto (see Table 13.2), one could impose the exact constraint that J_2 is 10/3 of C_{22} and solve for only C_{22} from the data, not both J_2 and C_{22}. This approach motivates the discussion below although it is not the approach we used in determining the values of J_2 and C_{22} used in Table 13.2. We actually imposed the 10/3 relationship as an *a priori* constraint, and let the data determine both J_2 and C_{22}, along with their correlation μ.

The correlation between J_2 and C_{22} can be interpreted in terms of a satellite's rotational and tidal response. The two parameters for the rotation and tide are defined by the single Love number k_f multiplied by the two small parameters q_r for the rotation and q_t for the tide. For the first-order theory of figures, the relationship between these two response parameters and the gravity coefficients is linear, and it is given by (see Eq. 13.10),

$$\begin{aligned} k_f q_r &= -3\,(2C_{22} - J_2) \\ k_f q_t &= -12 C_{22} \end{aligned} \quad (13.3)$$

A linear covariance analysis for the system of Eq. (13.3) yields an expression for the correlation μ_f between $k_f q_r$ and $k_f q_t$. It is a function of the correlation coefficient μ between J_2 and C_{22}, and the standard errors σ_J for J_2 and σ_C for C_{22}. It can be written as,

$$\mu_f = \frac{\mu\sigma_J - 2\sigma_C}{\sqrt{\sigma_J^2 - 4\mu\sigma_J\sigma_C + 4\sigma_C^2}} \quad (13.4)$$

From the gravity coefficients and their correlation in Table 13.2, the value of μ_f is 1.0 for Ganymede, 0.95 for Europa and Callisto, and -0.14 for Io. For the *Galileo* mission, the determination of the tidal and rotational coefficients is independent only for Io. As a result, Io's derived normalized axial moment of inertia, C/MR^2 is at least a factor of 10 more accurate than for the other three Galilean satellites.

The magnitude of the static distortion for a body deformed by rotation and tides is determined by the ratio of the equatorial centrifugal force to the gravitational force at the satellite's surface, or by the small parameter q_r given by

$$q_r = \frac{\omega^2 R^3}{GM} \quad (13.5)$$

* Nonsynchronous rotation of their figures with respect to the tidal axis on a geological timescale, as may be occurring for Europa (Chapter 15), does not affect our arguments.

where ω is the angular frequency for both the mean orbital period and the corresponding synchronous rotation. The satellite takes the shape of a triaxial ellipsoid with dimensions a, b, and c ($a > b > c$). The long axis of the ellipsoid is along the planet–satellite line and the short axis is parallel to the rotation axis. The distortion of the satellite depends on the magnitude of the rotational and tidal forcing and the distribution of mass with radius inside the body. The distortion of the satellite and its internal mass distribution determine the satellite's gravitational field.

The principal quadrupole gravitational coefficient C_{22} is related to the difference in the equatorial moments of inertia by (Kaula 1968),

$$C_{22} = \frac{B - A}{4MR^2} \tag{13.6}$$

where the ellipsoidal satellite's principal moments of inertia are A, B, and C ($C > B > A$). For a body in rotational and tidal equilibrium, the gravity coefficient C_{22} is related to the rotational response parameter q_r by

$$C_{22} = \frac{1}{4} k_f q_r \tag{13.7}$$

where the fluid Love number k_f depends on the distribution of mass within the satellite ($k_f = 3/2$ for constant density). Given C_{22} (or equivalently J_2) and q_r, k_f can be determined from Eq. (13.7), and the satellite's axial moment of inertia C follows from the Radau relationship (Kaula 1968),

$$\frac{C}{MR^2} = \frac{2}{3}\left[1 - \frac{2}{5}\left(\frac{4 - k_f}{1 + k_f}\right)^{1/2}\right] \tag{13.8}$$

The inferred axial moment of inertia provides a direct constraint on the internal mass distribution. This second constraint equation is

$$\bar{\rho}\left(\frac{C}{MR^2}\right) = \frac{2}{5}\left[\rho_s + (\rho_c - \rho_m)\left(\frac{r_c}{R}\right)^5 + (\rho_m - \rho_s)\left(\frac{r_m}{R}\right)^5\right] \tag{13.9}$$

For the three-layer model, there are two equations (Eq. 13.1 and Eq. 13.9) in five unknowns (r_c, r_m, ρ_c, ρ_m, ρ_s), but the situation is improved substantially by the measured moment of inertia. For example, if densities are assumed for the three layers, both the core radius and mantle radius become knowns. For the two-layer model, an assumption on shell density, for example ice or rock, yields both the core density and core radius from the two constraints. Alternatively, a forward modeling approach can be used to produce a suite of possible two- and three-layer interior models that satisfy the given constraints for radius, density, and moment of inertia.

The equilibrium parameters for the four Galilean satellites are given in Table 13.1. The rotation parameter q_r in Table 13.1 is computed from Eq. (13.5), and k_f is computed from Eq. (13.7) for synchronous rotation (the determination of C_{22} is discussed below). The mean density uses a mass inferred from the measured GM divided by the gravitational constant G ($6.672\,59 \times 10^{-20}$ km^3 s^{-2} kg^{-1}) (Cohen and Taylor 1999).

It is useful to check the equilibrium theory with known values of C/MR^2 for the rapidly rotating planets Earth and Mars. From the first-order theory of figures, the gravity coefficients J_2 and C_{22} are given in general by Hubbard and Anderson (1978),

$$\begin{aligned} C_{22} &= -\frac{1}{12} k_f q_t \\ J_2 &= \frac{1}{3} k_f \left(q_r - \frac{1}{2} q_t\right) \end{aligned} \tag{13.10}$$

where Hubbard and Anderson's (1978) dimensionless response coefficient α has been replaced by the fluid Love number $k_f = 3\alpha$, and q_t is the tidal coefficient

$$q_t = -3\left(\frac{R}{a_J}\right)^3 \frac{M_J}{M} \tag{13.11}$$

with a_J the distance to the tide-raising body and M_J its mass. For a body in synchronous rotation, $q_t = -3q_r$ (O'Leary and van Flandern 1972), and Eq. 13.7 is recovered. Similarly,

$$J_2 = \frac{5}{6} k_f q_r \tag{13.12}$$

which proves that J_2 is exactly 10/3 of C_{22} for synchronous rotation.

When the figure is distorted by rotation only, as in the case of Earth and Mars, both q_t and C_{22} are zero. It follows from Eq. 13.10 that

$$k_f = \frac{3J_2}{q_r} \tag{13.13}$$

With q_r equal to 0.003 449 8 for the Earth and J_2 equal to 0.001 082 6 (Schubert and Walterscheid 2000), equilibrium theory yields a value for k_f equal to 0.9415 and C/MR^2 from Eq. (13.8) is 0.3320. The value of k_f for the Earth's actual density profile is 0.937 (Stacey 1992), in quite good agreement with the equilibrium value. For Mars with q_r equal to 0.004 570 2 and J_2 equal to 0.001 964 (Tholen *et al.* 2000), the equilibrium value of k_f is 1.2869 and C/MR^2 is equal to 0.3762. The moment of inertia for Mars can be obtained independently from polar precession. A *Viking* lander result yields a value of C/MR^2 equal to 0.355 ± 0.015 (Yoder and Standish 1997), while a more recent combined *Viking* lander and *Pathfinder* lander result yields $C/MR^2 = 0.3662 \pm 0.0017$ (Folkner *et al.* 1997). The agreement with the equilibrium value is not as good as for Earth because of the uncompensated portion of the Tharsis uplift, but the good agreement with the independently determined value of C/MR^2 for the Earth, but less so for Mars, serves as a useful illustration and check on the equilibrium method.

13.2.1 Flyby Determination of C_{22}

The general gravitational potential of Eq. (13.2) can be simplified for an equilibrium body by first recognizing that for purposes of modeling the *Galileo* Doppler data, the third degree coefficients will be zero by symmetry and the fourth degree coefficients will be proportional to q_r^2 and completely negligible. The potential can be truncated at the second degree quadrupole terms. Among the five second-degree coefficients only J_2 and C_{22} are stimulated by the rotation and tides with $J_2 = (10/3)\,C_{22}$. Other coefficients might be included in the fitting model for purposes of trimming up the orientation of the principal axes or for studies of systematic error or additional signal, for example from gravity anomalies, but the equilibrium potential obtained from Eq. (13.2) is simply

Table 13.1. Equilibrium parameters.

Body	q_r (10^{-6})	k_f	R (km)	$\bar{\rho}$ (kg m^{-3})	C/MR^2
Io	1713.7	1.3043 ± 0.0019	1821.6 ± 0.5	3527.5 ± 2.9	0.378 24 ± 0.000 22
Europa	501.9	1.048 ± 0.020	1565.0 ± 8.0	2989 ± 46	0.346 ± 0.005
Ganymede	190.3	0.804 ± 0.018	2631.2 ± 1.7	1942.0 ± 4.8	0.3115 ± 0.0028
Callisto	37.0	1.103 ± 0.035	2410.3 ± 1.5	1834.4 ± 3.4	0.3549 ± 0.0042

$$V_{eq} = \frac{GM}{r}\left[1 + \frac{2}{3}\frac{C_{22}R^2}{r^4}\left(7x^2 - 2y^2 - 5z^2\right)\right] \tag{13.14}$$

where the cartesian x, y, z axes are aligned along the principal moments of inertia, with the x axis directed from the satellite to Jupiter and the z axis along the positive rotational axis. The radius r is just the modulus of the cartesian position vector (x, y, z). Actually, the potential is rotating with the satellite in inertial space, giving rise to Coriolis and centrifugal forces that must be taken into account for the real data analysis. However, for purposes of discussion, we ignore the rotational terms in the flyby trajectories and compute the acceleration components from the gradient of Eq. (13.14). The quadrupole part of the acceleration is (in vector components)

$$\boldsymbol{a}_2 = -\frac{GMC_{22}R^2}{r^7}\left[x(7x^2 - 8y^2 - 13z^2),\right.$$
$$\left. y\,(13x^2 - 2y^2 - 7z^2), 5z(3x^2 - z^2)\right] \tag{13.15}$$

It follows that to the first order in C_{22}, the magnitude of the total acceleration is

$$|\boldsymbol{a}| = \frac{GM}{r^2}\left[1 + 2C_{22}\left(\frac{R}{r}\right)^2\left(7\hat{r}_x^2 - 2\hat{r}_y^2 - 5\hat{r}_z^2\right)\right] \tag{13.16}$$

where $\hat{r}_x$, $\hat{r}_y$, $\hat{r}_z$ are the direction cosines for the spacecraft position. In terms of latitude ϕ and longitude λ, the acceleration is

$$|\boldsymbol{a}| = \frac{GM}{r^2}\left[1 + C_{22}\left(\frac{R}{r}\right)^2\left[5\left(3\cos^2\phi - 2\right)\right.\right.$$
$$\left.\left. +9\cos^2\phi\cos 2\lambda\right]\right] \tag{13.17}$$

The term in brackets containing the latitude and longitude scales as a simple r^{-4} power law for the quadrupole acceleration. It has a minimum of -10 at the pole and a maximum of 14 on the equator along the satellite–Jupiter line ($\lambda = 0$ or 180°). The zero crossings, where there are no acceleration signals, occur at latitudes below ±49.8° along a surface line given by

$$\cos 2\lambda = \frac{5\left(2 - 3\cos^2\phi\right)}{9\cos^2\phi} \tag{13.18}$$

For polar flybys, with closest approach near the pole, a nonzero acceleration is guaranteed, although it must be projected along the Jupiter–Earth line of sight. These considerations can be used to optimize flybys for a C_{22} determination, but in fact, the only real control over the *Galileo* flybys was to minimize the flyby distance and to make sure the spacecraft could be tracked in a coherent Doppler mode during the closest approach. However, for Ganymede, the mission plan included both an equatorial and a polar close flyby on the first and second orbits, an optimum plan for independently determining the rotational and tidal response of the satellite. After the end of the regular mission, Io flybys were planned, with a polar pass on orbit 25. For Europa and Callisto, all flybys were nearly equatorial, with the result that only a single gravity coefficient (C_{22}) could be determined, along the lines of Eq. (13.17).

For Doppler tracking, the measure of noise is the Allan deviation σ_y (Iess *et al.* 1999), which is proportional to the standard error σ_a in acceleration. The relationship is $\sigma_a = c\ \sigma_y/\tau$, where τ is the time interval over which the Doppler cycle counts are accumulated. For *Galileo*, σ_y is about 7×10^{-12}, including both random and systematic error, at solar elongation angles greater than 90° and for τ equal to 1000 s. Therefore, the expected error in a C_{22} acceleration measurement is about $\sigma_a = 2 \times 10^{-6}$ m s^{-2}. From Eq. (13.16) or Eq. (13.17), the quadrupole acceleration on a close flyby will fall between the approximate limits of 1 to 10 times $GMC_{22}R^{-2}$. The acceleration of gravity GMR^{-2} varies between the limits of 1.236 m s^{-2} for Callisto and 1.796 m s^{-2} for Io. Consequently, with consideration of the factor of 10, and also the much smaller variation in GMR^{-2}, the expected error on C_{22} in units of 10^{-6} varies between the limits of about 0.11 to 1.6. The results from *Galileo* do indeed fall within these limits, except for Europa with a standard error of 2.5×10^{-6}.

13.2.2 Gravity Results

Io

The best published Io results (Anderson *et al.* 2001b) are based on four close flybys. There is also a more recent close flyby on 17 January 2002, which can be analyzed for improved results. Unfortunately, on that last Io flyby of the *Galileo* mission, the *Galileo* spacecraft automatically shut down the science sequence in response to the detection of a possible fault. However, Doppler tracking with the S-band radio carrier wave proceeded as scheduled. As a result, a total of four close Io flybys are available for gravity analysis with *coherent* Doppler data, orbit numbers I24 (11 Oct 1999), I25 (26 Nov 1999), I27 (22 February 2000), and I33 (17 Jan 2002). The first close flyby before Jupiter Orbital Insertion (JOI) in December 1995 is also available, but the spacecraft was tracked in a one-way mode with the Doppler measurements referenced to the spacecraft oscillator, not the DSN atomic frequency standards used for coherent Doppler. Although this first flyby was the basis for the detection of a large metallic core in Io (Anderson *et al.* 1996b), and although it has been retained in the Io data set, it adds little C_{22} information to the four later flybys. The closest of the five flybys in the data set is the last on the 33rd orbit at 102 km altitude, followed by a flyby on the 27th orbit at 198 km altitude and a polar flyby on the 25th orbit at 300 km altitude. A combination of data from this polar pass with the other four equatorial passes can be used to ob-

Table 13.2. Gravity results from the *Galileo* mission.*

Body	GM (km^3 s^{-2})	J_2 (10^{-6})	C_{22} (10^{-6})	μ
Io	5959.91 ± 0.02	1859.5 ± 2.7	558.8 ± 0.8	0.472
Europa	3202.72 ± 0.02	435.5 ± 8.2	131.5 ± 2.5	0.993
Ganymede	9887.83 ± 0.03	127.53 ± 2.9	38.26 ± 0.87	1.000
Callisto	7179.29 ± 0.01	32.7 ± 0.8	10.2 ± 0.3	0.997

*See Table 13.1 for the reference radius associated with J_2 and C_{22}. The GM values are from Jacobson (2002). μ is the correlation coefficient between J_2 and C_{22}.

tain an independent determination of rotational and tidal terms in the gravitational potential. The addition of data from the last 102 km flyby reduces the error on the gravity coefficient C_{22} by about 30% over what we previously reported from four flybys (Anderson *et al.* 2001b), and it also reduces the correlation between J_2 and C_{22} from 0.752 to 0.472. The final results of our *Galileo* collaboration (Anderson *et al.* 2002) from a complete set of Io data are given in Tables 13.1 and 13.2. These final values are reasonably consistent with previous results (Anderson *et al.* 1996b, 2001b), and they definitely satisfy the equilibrium constraint that $J_2 = (10/3)C_{22}$. The difference between the previous value of C_{22}, 553.7 ± 1.2, in units of 10^{-6}, which excludes the excellent data from I33, and the C_{22} in Table 13.2, 558.8 ± 0.8 (in units of 10^{-6}), which includes I33, is 4.25σ. This translates into a difference in C/MR^2 of 4.0σ. This is certainly not an insignificant difference, and it indicates that further analysis of the complete Io data set might yet be undertaken. The quoted errors represent realistic errors, including both random and systematic error, hence a difference of 4.25σ in C_{22} is disturbing. The difference probably arises from an extraordinarily large Io ephemeris error, perhaps amplified by the relatively large time interval between I33 and the more closely spaced flybys I24, I25, and I27. An improvement in the Io ephemeris could reconcile the difference that arises from adding in the closest I33 flyby. Until that analysis is carried out, we recommend using the results in Tables 13.1 and 13.2 as the final *Galileo* results for Io gravity.

Europa

All available Europa flybys have been analyzed and the results have been published (Anderson *et al.* 1998b). The first encounter occurred on the 4th orbit at an altitude of 697 km, the second on the 6th orbit at an altitude of 591 km, the third on the 11th orbit at an altitude of 2048 km, and the fourth on the 12th orbit at an altitude of 205 km. There was some concern that the Europa ionosphere, detected by the *Galileo* radio occultation experiment (Kliore *et al.* 1997), might imply a neutral atmosphere that could introduce drag perturbations into the flyby trajectory. No drag perturbations were detected, however, which is consistent with estimates of the surface density of 5×10^{-12} kg m^{-2}, about six times too small for a drag detection with the *Galileo* spacecraft. The gravity results are shown in Table 13.2. There is a small bias of 0.5×10^{-6} in C_{22} because of difficulties with defining the Europa–Jupiter direction (Anderson *et al.* 1998b), but the bias is a factor of five smaller than the standard error, hence of little concern. The high correlation between J_2 and C_{22} is the result of all four flybys being nearly equatorial. It is impossible from the data to separate Europa's tidal and rotational responses, but the relatively large forcing, as evidenced by q_r in Table 13.1, suggests strongly that the quadrupole gravity field is a true reflection of an interior in hydrostatic equilibrium.

Ganymede

Like Europa, all Ganymede flybys are finished, but unlike Europa the data analysis is not complete. The published results from two Ganymede flybys on the first two orbits, however, still represent the best estimate of Ganymede's equilibrium field (see Table 13.2) (Anderson *et al.* 1996a). The first flyby was a near-equatorial pass at an altitude of 835 km, while the second was a near-polar pass at an altitude of 261 km. Two additional flybys on the 7th and 29th orbits provide additional gravity information by means of reasonably close encounters with coherent Doppler data, but the problem with the data analysis is that a gravity field complete through degree and order four is required in order to fit the data to the noise level. Further, without the equilibrium constraint $J_2 = (10/3)\ C_{22}$, the independently determined coefficients are unphysical. This makes the expected independent determinations of rotational and tidal components impossible. Problems with the Ganymede data analysis can be alleviated by assuming that the truncated field at the fourth degree can be interpreted in terms of a positive gravity anomaly in the vicinity of the closest approach on the second orbit ($\phi = 79.29°$, $\lambda = 123.68°$ west) (Anderson *et al.* 2001a). Independent of the gravity analysis, the analyses of images of Ganymede's limb yield a physical mean radius of 2631.2 ± 1.7 km. The imaging data reveal no significant deviations from sphericity.

The new data analysis yields a GM for Ganymede of 9887.83 ± 0.03 km^3 s^{-2}. The uncertainty in the gravitational constant G has increased in recent years as a result of inconsistent laboratory measurements (Cohen and Taylor 1999), but because of the improved value of mean radius, Ganymede's mean density is a factor of 4.6 more accurate than reported in 1996. The new mean density is 1942.0 ± 4.8 kg m^{-3}. Work is in progress to characterize the size and distribution of the gravity anomaly that apparently perturbs the equilibrium field.

Callisto

Five Callisto flybys have yielded final results for that satellite (Anderson *et al.* 2001c). Although there was some initial

confusion early in the mission over whether the gravity coefficients implied that Callisto was undifferentiated or partially differentiated, a complete separation of rock and ice was definitely ruled out. The final results (Table 13.2) argue for partial separation (see Section 13.6). Also the mean radius is 2410.3 ± 1.5 km, which yields a mean density of 1834.4 ± 3.4 kg m^{-3}. All five Callisto flybys were nearly equatorial, hence an independent determination of the tidal and rotational components of Callisto's gravitational field is impossible.

13.3 IO – INTERIOR MODELS

The gravity data of the previous section show that Io possesses an iron-rich core. At least the outer part of the core should be molten (e.g., McEwen *et al.* 1989). The radius and mass of the core and its composition remain uncertain, however. Io's mean density of 3527.5 kg m^{-3} (Table 13.1) suggests that it consists of silicates and iron. As discussed above, Io's normalized moment of inertia is $0.376\,85 \pm 0.000\,35$ (Table 13.1). The independent determination of the quadrupole coefficients J_2 and C_{22} using all four *Galileo* flybys is consistent with Io being in hydrostatic equilibrium, although the observed ratio of 10/3 between J_2 and C_{22} does not *sensu strictu* require hydrostatic equilibrium. If it is assumed that Io's core consists of pure iron with a density of around 8090 kg m^{-3}, then the core with a radius of about 650 km (solve Eq. (13.1) and Eq. (13.9) with $\rho_m = \rho_s$) comprises about 10% of the satellite's mass; if the core consists of a eutectic Fe–FeS alloy with a density of 5150 kg m^{-3}, then the core radius is about 950 km and the mass fraction is about 20% (see also Anderson *et al.* 1996b, 2001b, Kuskov and Kronrod 2001b, Sohl *et al.* 2002). Because the core radius and mass fraction also depend on the temperature in Io (Sohl *et al.* 2002) these estimates are uncertain at the 10% level.

Models of Io's static tidal deformation (Segatz *et al.* 1988) have provided a similar assessment of interior structure. The ratio of the $(b-c)$ to $(a-c)$ differences between the major figure axes can be used as a measure of the closeness to hydrostaticity, similar to the ratio between J_2 and C_{22}. The fluid tidal Love number h_f can be calculated from the axes if hydrostatic equilibrium is assumed. The Love number h_f measures the interior density distribution just as C/MR^2. Segatz *et al.* (1988), using *Voyager* limb measurements, found that Io is close to hydrostatic equilibrium and, assuming that the core is composed of a eutectic Fe–FeS alloy and a mantle whose composition and mineralogy and thus density are similar to that of the Earth's upper mantle, calculated a core radius of about 950 km. They find h_f of their model close to the value calculated from the figure axes. *Galileo* limb measurements (Thomas *et al.* 1998) and photogrammetric triangulation (Davies *et al.* 1998, Archinal *et al.* 2001) have recently confirmed Io's hydrostatic shape.

A substantial iron-rich core is also expected from cosmochemical considerations (e.g., Consolmagno 1981). Although the exact composition of the core is not known, it is possible, if not likely, that the core is rich in sulfur. The abundances of elemental sulfur and SO_2 on the surface of Io suggest that the primordial composition and oxidation state of Io was close to that of a volatile-depleted, metal-free CV or CM chondrite (Consolmagno 1981, Lewis 1982). The elemental abundance of sulfur would then be about 2–3 weight % of the entire satellite. Consolmagno (1981) points out that this amount of sulfur may be present either near the surface, where it would form a 20–30 km thick crust, or in the core, which could then have a closer to eutectic composition. A 20–30 km thick sulfur crust is incompatible with surface elevations of 10 km (e.g., Carr *et al.* 1998b), judging from the rheology of sulfur. By modeling Io as an olivine-dominated mantle and an Fe–FeS core, Sohl *et al.* (2002) find the Fe/Si ratio to be between 1 and 1.25 for models of Io with a solid mantle (values increasing with increasing temperature) and between 1.25 and 1.5 for a partially molten mantle. These values are smaller than the value of 1.7 typical of CI or CM chondrites (Lodders and Fegley 1998, pp. 314–316); the values are more consistent with those of CV chondrites.

Kuskov and Kronrod (2001b) have done a more complete study of the possible composition of Io by using the mass and moment of inertia data and matching possible density structures to the compositions of candidate carbonaceous and ordinary chondritic meteorites. For the core, these authors assume pure Fe, eutectic Fe–FeS (22.5 weight-% S), or troilite (FeS). In addition to the Fe/Si ratio, these authors calculate the ratio between Fe in the metal phase (including FeS), Fe_m, and the total Fe content, Fe_{tot}. They obtain permissible Fe/Si ratios of 0.8–1.2 and Fe_m/Fe_{tot} ratios of 0.36–0.55. The differences in the Fe/Si ratios from the values of Sohl *et al.* (2002) may in part be due to a more realistic mantle model and in part be due to lack of information on partial melting. In any case, Kuskov and Kronrod (2001b) conclude that their Fe_m/Fe_{tot} values are inconsistent with carbonaceous chondritic compositions but consistent with the compositions of ordinary L and LL chondrites which also have Fe/Si ratios that better fit their model (L and LL chondrites have Fe/Si ratios of 1.17 and 1.05, respectively).

To supply the surface heat flow of 2.5 W m^{-2} (Veeder *et al.* 1994, Spencer *et al.* 2000) or even larger values (Matson *et al.* 2001) by tidal dissipation in Io's silicate mantle requires at least a molten outer core layer; the volcanic activity, resurfacing rate and high temperature lava (1700 to 2000 K) (McEwen *et al.* 1998a,b, 2000, Lopes-Gautier *et al.* 1999) suggest that Io's mantle is partially molten. Keszthelyi *et al.* (2003) build on the low iron chondritic model of Kuskov and Kronrod (2001b) and use the evidence from the *Galileo* SSI and NIMS data for very high lava temperatures and othopyroxene-rich compositions to calculate the degrees of partial melting in the lava source regions of about 50%. A molten outer core layer is necessary if sufficient flexing of the mantle is to explain the observed luminosity through tidal heating. This was first pointed out by Peale *et al.* (1979) and later confirmed for more realistic models of Io's interior structure and rheology by Segatz *et al.* (1988). The mantle partial melt could be concentrated in an asthenosphere channel and/or distributed more evenly throughout the mantle. Both tidal dissipation in a low viscosity, asthenosphere channel beneath the lithosphere and in a partially molten mantle can explain the infrared luminosity (Segatz *et al.* 1988). The asthenosphere would have a viscosity of 10^8–10^{12} Pa s (Segatz *et al.*, 1988, but see Spohn (1997) for correction of an error in Segatz *et al.* (1988) involving a factor of 2π in the forcing frequency) and a thickness between 10 km and 100 km. While the asthenosphere dissipation model does not

require partial melting, the low value of the inferred viscosity actually suggests a substantial degree of partial melting. The mantle dissipation model requires a viscosity between 10^{12} and 10^{16} Pa s (Spohn 1997). These values are smaller than a suggested value for the minimum viscosity of solid rock of around 10^{17} Pa s and therefore again imply partial melting, albeit with a smaller degree of melting.

Ross *et al.* (1990) have tried to fit the large-scale topography from *Voyager* data (Gaskell *et al.* 1988) to the figures of Io calculated from the asthenosphere dissipation model and the whole mantle dissipation model of Segatz *et al.* (1988). They found that the topography is best fit if 2/3 of the dissipation occurs in an asthenosphere and 1/3 in the mantle below the asthenosphere. However, the belt of topographic swells and lows along the equator observed by Gaskell *et al.* (1988) have not been confirmed by the more accurate *Galileo* data (Thomas *et al.* 1998). Nevertheless, *Galileo* imaging data confirmed a preferential concentration of hot spots and volcanic vents along the equator (Lopes-Gautier *et al.* 1999), also consistent with asthenosphere heating and asthenosphere heat transfer (Tackley *et al.* 2001). McEwen *et al.* (1998a) have speculated that Loki, Io's most powerful hot spot by far, might be fed by a deep mantle plume while the less powerful active volcanic centers might originate in the asthenosphere. Their spacing, and the spacing of those likely to have been active in the past century, is a few hundred kilometers, compatible with asthenosphere heat transport (Tackley *et al.* 2001).

Fischer and Spohn (1990) and Spohn (1997) have argued, on the basis of their integrations of the orbit evolution equations of Yoder (1979) and Yoder and Peale (1981), that Io must be partially molten if locked in a stable near-equilibrium state with a sufficiently large dissipation rate. In such a state, surface heat flow is approximately balanced by tidal dissipation and the cooling rate is very small. At sufficiently large, but still subsolidus temperatures, the tidal dissipation rate E will be inversely proportional to the viscosity μ. The convective heat transfer rate q will be inversely proportional to μ^{β}, where β is about 0.3. Thus the ratio $(\mathrm{d}\ln E/\mathrm{d}T)/(\mathrm{d}\ln q/\mathrm{d}T) \approx \beta^{-1} > 0$ and an equilibrium will be unstable. A slight increase in temperature will lead to runaway heating since the dissipation rate will increase more rapidly than the heat transfer rate. A slight decrease in temperature will lead to runaway cooling. Above the solidus, the dissipation rate decreases rapidly with increasing temperature because the shear modulus decreases rapidly with increasing degree of partial melting. The heat transfer rate will largely continue to increase with temperature. As a consequence, $(\mathrm{d}\ln E/\mathrm{d}T)/(\mathrm{d}\ln q/\mathrm{d}T) < 0$ and an equilibrium state will be stable. A positive fluctuation in temperature will lead to a decrease in dissipation rate and to an increase in heat transfer rate and vice versa for a negative temperature fluctuation. The tidal forcing period for Io is close to but larger than the Maxwell time based on reasonable rheologies and temperatures.

In Figure 13.2 we present a reasonable iotherm from Spohn (1997) that features an asthenosphere and a partially molten underlying mantle. The figure also shows the solidus of dry peridotite (a likely candidate for the mantle of Io) and a possible range of core liquidi. The solidus and the 40% melting line are taken from Takahashi (1986, 1990);

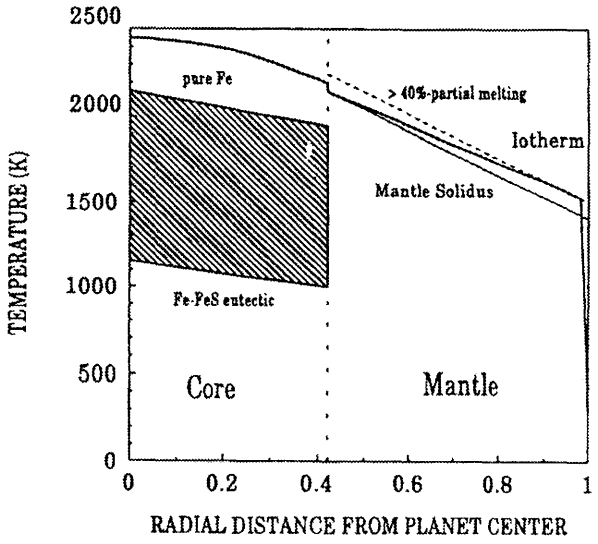

Figure 13.2. Thermal structure of the interior of Io. Plotted are a simplified mantle solidus based on the solidus of dry peridotite (Takahashi 1986, 1990), a line of constant 40% degree of partial melting after Wyllie (1988), a range of core liquidi between the pure iron liquidus and the liquidus of a eutectic Fe–FeS mixture (Usselman 1975b,a, Boehler 1986, 1992) and an Iotherm. The Iotherm follows the wet adiabat in the lower mantle, a constant degree of partial melting in the asthenosphere, and the adiabat in the core (see text). The steep near-surface gradient indicates the lithosphere.

the core liquidi have been derived by integrating the data of Usselman (1975b,a) and Boehler (1986, 1992).

In the core, the iotherm follows the adiabat. The core adiabat has been calculated using the parameter values for small planets given by Stevenson *et al.* (1983). In the mantle, the iotherm coincides with the solidus temperature at the core–mantle boundary and follows the wet adiabat (Turcotte 1982, Turcotte and Schubert 2002, Chapter 19) given by,

$$\frac{\mathrm{d}T}{\mathrm{d}p} = \frac{L}{c_{\mathrm{m}}}\frac{\mathrm{d}f}{\mathrm{d}p} \tag{13.19}$$

(T is temperature, p is pressure, L is the latent heat of mantle melting, c_{m} is the mantle specific heat at constant pressure, and f is the degree of partial melting) until it hits the 40% degree-of-partial-melting isoline. This degree of partial melting is consistent with the viscosity required for the asthenosphere tidal heating model. It is also about the maximum degree of partial melting at which the solid matrix still dominates the properties of the partial melt. At larger degrees of partial melting, large-scale melt segregation through vertical fluid transport is expected and would render the asthenosphere unstable.† Moreover, the observed topography seems to rule out the existence of an extremely low viscosity (<100 MPa s) melt layer beneath the lithosphere (Webb and Stevenson 1987), but collapsing mountains (Schenk *et al.* 2001a) argue that major rheological weakness in the asthenosphere (some level of mushiness) exists. The quantity $\mathrm{d}f/\mathrm{d}p$ has been estimated by linearly

† And indeed, asthenospheric stability at <40% partial melt remains an important open issue (Stevenson 2002).

interpolating between the solidus and the liquidus. In the asthenosphere, the iotherm follows the constant degree of partial melting line. In the lithosphere, the temperature gradient is steep enough to approximately balance, by heat conduction, a heat flow of 10^{13} W from the underlying mantle, about 1/10 of the observed heat flow of 10^{14} W.

The thickness of the lithosphere is only 25 km in the model of Figure 13.2. If the heat flow were balanced entirely by heat conduction, the lithosphere would have to be as thin as a few kilometers. These values of lithosphere thickness are inconsistent with the ~10 km heights of mountains on Io (Carr *et al.* 1998b, Schenk *et al.* 2001b). Pratt isostasy would require substantially thicker lithospheres of about 100 km thickness. However, it is likely that this is an upper limit to lithosphere thickness since the models of Segatz *et al.* (1988) have shown that the dissipation rate decreases strongly for thicker lithospheres. The conclusion drawn from these considerations is that magma must transfer most of the heat across the lithosphere. Magmatic heat transport permits a less steep temperature gradient and a lithosphere thickness consistent with the heights of the mountains (O'Reilly and Davies 1981). Heat conduction through the entire lithosphere cannot make a major contribution to the surface energy balance. This is important because it has often been thought that the remotely observed heat flow might severely underestimate Io's total surface heat loss because of the unknown contribution of conductive heat flow (but see Stevenson and McNamara 1988). Moore (2001, 2003) and Monnereau and Dubuffet (2002) have modelled magma heat transport through Io's lithosphere and concluded that even smaller degrees of partial melting than in the model of Figure 13.2 suffice to transfer all of Io's tidally generated heat.

It is possible that Io's lithosphere is compositionally different from the underlying mantle, e.g., it may coincide with a crustal layer of basaltic composition (Ross *et al.* 1990), and its thickness may not depend simply on the temperature gradient but also on the rates of basalt production and, possibly, recycling. The observed high lava temperatures of 1700 to 2000 K (McEwen *et al.* 1998b) have been used to suggest that the lava may be komatiitic and that the present Ionian crust may resemble the Earth's Archean crust.

As Figure 13.2 shows, the solidus temperature of the mantle at the core–mantle boundary is significantly larger than even the liquidus temperature of pure iron. Although the liquidus is steeper than the core adiabat, the temperature in the center of the core is still superliquidus. This has an important consequence for a possible dynamo in the core. If Io's core is liquid, then the latent heat and the gravitational energy liberated by the redistribution of light elements in the core upon freeze out of an inner core are not available to drive an Ionian dynamo. Instead, a dynamo must be driven by thermal power alone; a purely thermal dynamo is much less efficient than a dynamo driven by compositional buoyancy (Gubbins *et al.* 1979, Stevenson *et al.* 1983). For the latter, the gravitational energy can be directly made available to drive the dynamo while a thermal dynamo is subject to a Carnot efficiency factor. Wienbruch and Spohn (1995) have argued that as long as Io is tidally heated in a stable, near equilibrium state, the surface heat flow will be approximately balanced by tidal dissipation, and satellite and core cooling will be negligible. This led them to suggest that Io would not have a magnetic field unless equilibrium between tidal heating and heat flow is substantially perturbed. The *Galileo* spacecraft's last flyby of Io, just 300 km above the north pole, failed to detect a magnetic field of internal origin (Kivelson *et al.* 2002a). The first close flyby of Io, just before insertion of the *Galileo* spacecraft into orbit around Jupiter, had detected magnetic field perturbations associated with either electrical currents in the plasma around Io or a dynamo inside the satellite (Kivelson *et al.* 1996b, Khurana *et al.* 1997a). Apparently, Io does not have a magnetic field (chapter by Kivelson *et al.*). Lack of adequate core cooling, as suggested by Wienbruch and Spohn (1995), is a plausible explanation. Additional discussion of the magnetic field measurements near Io can be found in Chapter 21 by Kivelson *et al.*

13.4 EUROPA – INTERIOR MODELS

Analyses of the radio Doppler data discussed earlier show Europa to most likely be a differentiated satellite consisting of a metallic core (mostly iron), a silicate mantle, and a water ice–liquid outer shell (Anderson *et al.* 1997, 1998b). The gravity data say nothing about the solidity or fluidity of the metallic core or outer water shell, and they do not uniquely determine the internal structure of Europa. For example, Europa's interior could consist of a uniform mixture of dense silicate and metal beneath the water ice–liquid outer shell. The inference of interior structure from the gravity data also rests on the assumption that Europa is in hydrostatic equilibrium. Interior models are constrained by Europa's average density of 2989 ± 46 kg m^{-3} (Table 13.1) and its gravitational coefficient $C_{22} = 131.5 \pm 2.5 \times 10^{-6}$ (Table 13.2). The uncertainty in Europa's density is mainly due to the stated 8 km uncertainty in the satellite's radius $= 1565 \pm 8$ km (Table 13.1) although more refined values are now available (Seidelmann *et al.* 2002, Table V). Europa's axial moment of inertia C, normalized by the product of its mass M and radius squared R^2, is 0.346 ± 0.005 (Table 13.1). This value of C/MR^2 is substantially less than 0.4, the value of C/MR^2 for a sphere of constant density, and it requires a concentration of mass toward the center of Europa.

Three-layer models of Europa's interior consistent with its average density and gravitational coefficient C_{22} are shown in Figure 13.3. A density of 1050 kg m^{-3} has been assumed for the outer water ice–liquid shell and two possibilities for the metallic core are considered, an Fe core of density 8000 kg m^{-3} (Figure 13.3A) and an Fe–FeS core of density 5150 kg m^{-3} (Figure 13.3B). The radius of Europa's metallic core is uncertain in part because of its unknown composition, i.e., the concentration of a light element such as sulfur in the core, and in part because of the unknown thickness of the water ice–liquid shell. The core radius could be as large as about 45% of Europa's radius (if the core composition is that of an Fe–FeS eutectic and if the water ice–liquid shell is about 100 km thick) or only as large as about 13% of Europa's radius (if the core is mainly Fe and if the water ice–liquid shell is 170 km thick) (Sohl *et al.* 2002). Since a uniform mixture of rock and metal beneath an outer water ice–liquid shell is consistent with the density and moment of inertia constraints for Europa, it is not possible to provide a rigorous lower bound on the radius of Europa's core. However, the density of such a mixture

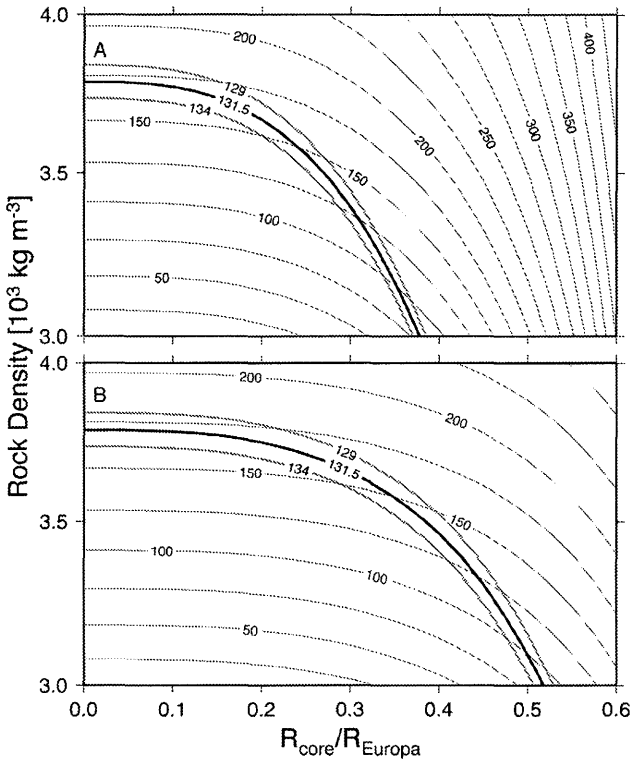

Figure 13.3. Three-layer models of Europa consisting of a water ice–liquid outer shell with density 1050 kg m^{-3}, a rock mantle, and either an Fe core of density 8000 kg m^{-3} (A) or an Fe–FeS core of density 5150 kg m^{-3} (B). In addition to the densities of the core and outer water ice–liquid shell, a model is completely specified by its values of rock density (vertical axis) and normalized core radius (horizontal axis). The contours labelled 129, 131.5, and 134 delineate models with the indicated values of C_{22} (in units of 10^{-6}). The other contours give the thickness (in km) of the outer water ice–liquid shell. Only those models with C_{22} values consistent with observation are plausible models of Europa. A core-free Europa model is possible only if the rock density is significantly greater than the density of bulk Io.

would have to exceed 3800 kg m^{-3}, requiring some enrichment in dense metallic phases relative to Io, which has a bulk density of 3529 kg m^{-3} and, likely, a hotter interior. Such degrees of enrichment in dense phases are probably unlikely for a smaller body forming farther out in the proto-jovian nebula than Io. It is more likely that this mixture would separate into a metallic core and rock mantle, because radiogenic heating in the silicates alone would raise Europa's interior temperatures high enough for differentiation to occur (Anderson *et al.* 1998b). Thus, while we cannot specify a minimum value for the radius of a metallic core in Europa, it is most likely that such a core exists.

The minimum water ice–liquid outer shell thickness is about 80 km for plausible mantle densities (Anderson *et al.* 1998b). Smaller outer shell thicknesses require mantle densities less than 3000 kg m^{-3}. Such small mantle densities are possible only if the mantle silicates are hydrated. In effect, the water in the outer shell trades off with the water in hydrated mantle silicates. If the mantle density is sufficiently small there is enough density contrast between the mantle and metallic core to account for the relatively small moment of inertia of Europa. Otherwise, a thick water ice–liquid shell (less than about 170 km thick) is needed to provide the requisite density contrast between the exterior and deep interior of Europa. Hydrated silicates break down and release their water at temperatures between 500 and 800°C at the pressures in Europa's interior, making it unlikely that a thick Europa mantle would have an average density less than about 3000 kg m^{-3}. Furthermore, it is implausible that Europa would have differentiated a metallic core while retaining a hydrated silicate mantle.

Sohl *et al.* (2002) have explored compositional models of Europa consistent with the mean density and moment of inertia constraints. They assume that Europa's core is composed of iron and sulfur and its mantle is made of forsterite and fayalite. Europa models with thick water ice–liquid outer shells have relatively small metallic cores that are rich in iron and mantles that have about equal amounts of forsterite and fayalite. As water ice–liquid shell thickness decreases, the mantle becomes more forsterite rich. There is a tendency for the size of the metallic core to increase with decreasing thickness of the water ice–liquid shell, but for any given shell thickness, there is a range of core radii corresponding to different core sulfur concentrations. The bulk Fe/Si ratio decreases with decreasing water ice–liquid shell thickness but it is almost independent of core radius and chemistry. A Europa model with a water ice–liquid shell about 170 km thick has a bulk Fe/Si ratio about equal to the CI carbonaceous chondrite value of 1.7 ± 0.1. Models with thinner shells have substantially sub-chondritic bulk Fe/Si with the Fe/Si ratio decreasing with decreasing water ice–liquid shell thickness.

While the gravity field measurements by the *Galileo* spacecraft cannot tell us about the liquidity or solidity of the metallic core and water ice–liquid outer shell, the *Galileo* magnetic field observations near Europa (Khurana *et al.* 1998, Kivelson *et al.* 1999, 2000, Zimmer *et al.* 2000) can address these questions. Europa has no detectable internal magnetic field (Schilling *et al.* 2003). Accordingly, the magnetic field observations provide no information about the physical state of the core; while an active core dynamo requires at least part of the core to be molten, the absence of dynamo action does not imply a solid core. Europa's core could be entirely liquid but nonconvecting, in which case a dynamo would not be operative in the core. A similar explanation could account for the absence of internal magnetic fields on Venus and Mars (Stevenson *et al.* 1983) and on Io, as discussed in the previous section.

The magnetic field observations are more definitive with regard to the physical state of the water ice–liquid outer shell. They show that the temporal variability of the jovian magnetic field, as sensed by Europa during its orbit around Jupiter, induces electric currents inside Europa. The induced electric currents in turn produce magnetic field fluctuations that were detected by the magnetometer on the *Galileo* spacecraft during several flybys of Europa. The magnitude of the induction-generated magnetic field fluctuations provides information on the electrical conductivity, depth, and thickness of the region in Europa where the induced electrical currents flow. The electrically conducting layer in Europa must lie within about 200 km of the surface and its electrical conductivity must be comparable to that of seawater on Earth if its thickness is at least several kilometers (Zimmer *et al.* 2000). This is strong, albeit indirect evidence

for a subsurface liquid salt water ocean in Europa's water ice–liquid outer shell. The constraints on the depth of the internal ocean from the magnetometer data are consistent with the estimate of the thickness of the water ice–liquid outer shell from the gravity data.

There is considerable indirect geologic evidence to support the existence of either a global liquid water ocean or layer of warm, soft, ductile, possibly partially melted ice beneath the surface of Europa (Carr *et al.* 1998a, Geissler *et al.* 1998, Pappalardo *et al.* 1998, 1999, Spaun *et al.* 1998, Sullivan *et al.* 1998, Hoppa *et al.* 1999, 2000, Greenberg *et al.* 2000, 1998, Tufts *et al.* 2000, Moore *et al.* 2001). The evidence includes the young apparent age of the surface, relaxation of large craters, the morphology of multi-ringed impact basins, mobile and tilted ice blocks, smooth deposits, chaotic terrain, strike-slip faulting, ridge morphology and distribution, and others. Global-scale tectonic patterns can be explained by nonsynchronous rotation and tidal flexing of a thin ice shell above a liquid water ocean (Geissler *et al.* 1998, Hoppa *et al.* 1999, Greenberg *et al.* 2000, Tufts *et al.* 2000). Some geologic features suggest that the internal ocean is within a few kilometers of the surface (e.g., Greenberg *et al.* 1998, Kattenhorn 2002). Other features suggest that the ocean lies beneath a few tens of kilometers of ice (e.g., Schenk 2002, Nimmo *et al.* 2003).

Thermal models of Europa can assess the likelihood of a liquid water ocean in Europa's water ice–liquid outer shell (Schubert *et al.* 1986, Spohn and Schubert 2003). Accretional and radiogenic heat sources are large enough to dehydrate Europa early in its evolution leaving the satellite covered with a layer of liquid water 100 km or more thick. Thermal models by Consolmagno and Lewis (1977) and Fanale *et al.* (1977) considered only the conductive cooling and freezing with time of the outer layer of water and predicted liquid water beneath an ice shell at present. However, Reynolds and Cassen (1979) and Cassen *et al.* (1979) showed that the outer layer of ice would become unstable to convection with sufficient thickening, thereby promoting heat transfer through the ice and the cooling and solidification of the underlying liquid water. Their models resulted in complete freezing of the outer layer of water in a small fraction of geologic time.

Subsolidus convection in a freezing and thickening ice layer is not as efficient as assumed by Reynolds and Cassen (1979) and Cassen *et al.* (1979). Because of the strong dependence of ice viscosity on temperature, convection in the outer ice layer occurs in the so-called stagnant-lid regime (Solomatov 1995). This is a style of convection in which the outermost layer of ice is too cold and stiff to participate in the convection and only the lower, more ductile layers of the ice convect. Heat transfer through the stagnant lid is by conduction, and only a fraction of the total temperature drop across the ice is available to drive convection (see McKinnon (1998) for a discussion). As a result, convection is less vigorous and the ice layer cools and thickens more slowly than it would if its viscosity were not strongly temperature dependent. This opens the possibility that the freezing of the outer water layer could occur so slowly that a liquid region would survive to the present. At the very least it would take longer for the outer water layer to freeze out completely.

The effect of stagnant-lid convection on the thermal evolution of icy satellites has been studied by Deschamps and Sotin (2001) and by Spohn and Schubert (2003). Deschamps and Sotin (2001) find that though the rate of freezing of the outer water layer is slowed by stagnant-lid convection, the layer is nevertheless completely frozen at present if the layer is pure H_2O and if the only source of heating the layer is radiogenic heating from the rocks in the satellite. Spohn and Schubert (2003) have considered wide ranges of parameter values and have included the effect of the strong gradient of the solidus on the rheology under the empirically justified assumption that the viscosity depends on the homologous temperature (this assumption is consistent with the measured negative activation volume for power-law creep of ice, Durham and Stern 2001). According to these calculations thin oceans cannot be completely ruled out even for pure H_2O ice shells because of uncertainties in the parameter values relating heat flow to the vigor of convection and because of the unknown contribution of satellite interior cooling to the energy balance of the ice shell. Convection is also more difficult to achieve if the ice rheology is non-Newtonian (Solomatov and Moresi 2000). This provides an additional mechanism to delay ocean freezing (Ruiz 2001). The effect of grain size on ice rheology is yet another factor that needs to be considered (Nimmo and Manga 2002).

There are several ways in which the freezing of Europa's internal ocean could be prevented. One of them is tidal heating. Cassen *et al.* (1979) included the heat produced by tidal dissipation in Europa's outer ice shell and found that this heat source could offset the subsolidus convective cooling of the ice and prevent complete solidification of the water ocean. A steady state could be achieved in which tidal dissipative heating in an ice shell above a liquid water ocean is carried upward by convection in the ice; the balance between the dissipative heat source and the convective cooling leaves the ice layer with a constant thickness. Cassen *et al.* (1980) later revised their estimate of tidal heating downward, again opening the question of whether the water layer on Europa would freeze completely over geologic time.

The competition between the tendency of tidal heating to maintain a liquid water ocean and that of subsolidus ice convection to freeze the ocean has been analyzed for nearly two decades (Squyres *et al.* 1983, Ross and Schubert 1987, Ojakangas and Stevenson 1989, Fanale *et al.* 1990, Yoder and Sjogren 1996). Hussmann *et al.* (2002) have coupled a Maxwell rheology model of tidal heating to a heat transport model including stagnant-lid convection. The thicknesses of the elastic and viscoelastic parts of the ice shell were calculated assuming equilibrium between tidal heating in the viscoelastic shell and the heat flow through the layers. The thickness of the ice layer should then be between 20 and 50 km depending on the rheology of the ice with 30 km being the most reasonable value. The surface heat flow is about 20 mW m^{-2}. Much larger tidal heating rates corresponding to heat flows up to a few 100 mW m^{-2} are, in principle, possible but only if the ice layer is thicker than the equilibrium thickness. The dissipation rate will then exceed the heat transfer rate which will result in thinning towards the equilibrium thickness.

A major complication in the thermal modeling of the water ice–liquid outer layer on Europa is the rheology of ice (Durham and Stern 2001, Durham *et al.* 1997, 1998, 2001, Goldsby and Kohlstedt 1997, 2001, Stern *et al.* 1997) both in its control of convection and dissipation. The phenomena

of dissipative heating and convective cooling involve nonlinear feedback mechanisms associated with the dependence of viscosity on temperature and the dependence of temperature on the heating and cooling mechanisms. The amount of tidal heating in the ice depends on the magnitude of tidal deformation and the rheology of the ice at tidal periods. The amount of tidal deformation in the ice shell depends on the internal structure, in particular the existence of a liquid ocean beneath the ice layer and the ice thickness.

There are additional uncertainties and effects that can be important in controlling the thermal history of the water ice–liquid outer layer. The thermal conductivity of the ice is dependent on temperature and physical state of the ice (density and distribution of cracks, for example). A thermally insulating layer at the surface of Europa would promote stabilization of a liquid water ocean (Ross and Schubert 1987, Spohn and Schubert 2003). The occurrence of minor constituents in the ice and ocean such as salts (McCord *et al.* 1998) and ammonia (Kargel *et al.* 1991, Deschamps and Sotin 2001) would affect the rheology of the ice and the freezing temperature of the ocean. By reducing the freezing temperature of the liquid, the presence of ammonia acts to lower the temperature of the ice thereby increasing its viscosity and reducing the vigor of convection (Deschamps and Sotin 2001). Through its direct reduction of the freezing point and its indirect effect on ice viscosity, the presence of ammonia or other volatiles in the liquid ocean acts to preserve the ocean. Tidal heating on major faults in Europa's ice shell may be important (Stevenson 1996a) and tidal heating due to forced circulations in a thin liquid water ocean sandwiched between the rock interior and the overlying ice may prevent complete solidification of the ocean (Yoder and Sjogren 1996). Tidal heating and the presence of ammonia or other volatiles or salts in the ocean are thus the most likely ways of preserving an internal ocean beneath the icy surface of Europa. We return to these issues in greater detail in Section 13.7.

A spacecraft orbiting Europa could determine with some confidence whether the moon has an internal liquid water ocean by measuring the gravitational or topographic amplitude of the semidiurnal (1.8 day) tide (Moore and Schubert 2000, Wu *et al.* 2001). The semidiurnal tide is superimposed on the much larger static tide that has been measured gravitationally by the *Galileo* spacecraft (Anderson *et al.* 1998b). The static tide reflects the behavior of Europa as an entirely fluid body over the billion year timescale on which the mean distance from Europa to Jupiter changes. The response of Europa to the semidiurnal tide, however, reflects the viscoelastic properties of Europa's interior on a timescale of a few days. This timescale is sufficiently short that competent solids like ice or rock behave differently from fluids, and Europa's semidiurnal tidal distortion will depend sensitively on whether Europa does or does not have an internal liquid water ocean. Moore and Schubert (2000) calculated the tidal response of Europa by solving the quasi-static equilibrium equations for a body composed of several uniform Maxwell viscoelastic layers. Models with no internal liquid water ocean were found to have a semidiurnal tidal distortion of only about a meter, while models with an internal ocean distort by about 30 m. The 30 m tidal distortion is characteristic of any model of Europa in which a fluid-like layer (water or mushy ice) decouples an outer ice shell from the interior. The amplitude of the semidiurnal tidal response really depends on the product of the ice thickness and the rigidity of the soft layer and there is a trade-off between the two quantities. The simultaneous measurement of the gravitational and topographic tidal amplitudes will help resolve this ambiguity.

13.5 GANYMEDE – INTERIOR MODELS

Ganymede's water-ice-rich surface, geological evidence of past resurfacing, and low density of 1942.0 ± 4.8 kg m^{-3} (Table 13.1) have long pointed to at least partial differentiation (rock from ice) of the satellite's interior (McKinnon and Parmentier 1986, Schubert *et al.* 1986). The *Galileo* spacecraft's orbital tour has provided information on Ganymede's gravitational field (Table 13.2), as discussed earlier.

Interpretation of Ganymede's second-degree gravity field as entirely due to a hydrostatic response to rotation and jovian tides yields a normalized moment of inertia $C/M_G R_G^2 = 0.3115 \pm 0.0028$ (Table 13.1, M_G and R_G are the mass and radius of Ganymede, respectively), the lowest known of any of the solid planets or satellites (Anderson *et al.* 1996a). Comparison of $J_2 = 127.53 \pm 2.9 \times 10^{-6}$ (Table 13.2, calculated from the measured C_{22} assuming hydrostaticity) with, e.g., the calculations based on three-layer structural models (ice over mixed ice + rock over a rock core, where rock means a solar mixture of rock + metal) in Mueller and McKinnon (1988, their Figure 4) immediately indicates that the separation of rock from ice in Ganymede is essentially complete. Moreover, the detection of a magnetosphere and magnetic field at Ganymede (Gurnett *et al.* 1996, Kivelson *et al.* 1996a, 1998) strongly implies that differentiation has proceeded farther, to formation of a three-layer structure, i.e., a water-ice shell, a rock mantle, and a metallic core (Schubert *et al.* 1996).

Analysis of *Galileo* magnetometer data from six flybys of Ganymede (Kivelson *et al.* 1996a, 2002b, and Chapter in this book) has sharpened the view of Ganymede's magnetic field. It is dominated by a dipole moment of $\approx$715 nT R_G^3, substantially larger than that of Mercury, and tilted by about 176° with respect to Ganymede's spin axis. Kivelson *et al.* (2002b) present two fits to the complete field, one an internal dipole and quadrupole field (eight components) and the other an internal dipole plus an induced component (four components). They prefer the latter because the fit is slightly better with only half the terms, plus Europa and Callisto have been clearly shown to have an induced response, most likely due to internal, salty (electrically conductive) water oceans (e.g., Zimmer *et al.* 2000). The strength of Ganymede's induced response requires a good conductor relatively close to the surface (i.e., it cannot be a metallic core), and a salty water layer (ocean) within Ganymede is thus also inferred (Kivelson *et al.* 2002b).

A remarkable aspect of Ganymede's magnetic field is the relatively low power in the quadrupole components. Whether using the dipole plus quadrupole fit or the dipole plus induced term fit (whose unfitted quadrupole terms would be even smaller), the ratio of quadrupole to dipole power is much lower than would be anticipated by scaling for a metallic core of the expected size (described below)

(Kivelson *et al.* 2002b). This is probably an important clue to the origin of Ganymede's magnetic field.

Ganymede's magnetic field could be due to either dynamo action, remanent magnetization, or magneto-convection (Schubert *et al.* 1996). Magneto-convection is a process by which an external field, imposed on a convecting, electrically conducting fluid, is modified and amplified to produce a new "perturbation field". The strength of the new field is generally of the same order as the external field, however, which for the jovian field at Ganymede is only ~100 nT, and so is unlikely to be the cause of the present dipole field (Kivelson *et al.* 1996a, Schubert *et al.* 1996).

Remanent magnetism in a ferromagnetic rock core has been examined in detail by Crary and Bagenal (1998). Even for model rock cores that have a high magnetic susceptibility because they are rich in magnetite (a possible jovian subnebula condensate, Prinn and Fegley 1981) an external jovian field cannot sufficiently magnetize a cooling rock core to account for the present dipole field. As the outer layer of the rock core cools below the Curie point for permanent magnetization in the presence of an internal field, and thickens, it imposes limits on the field strength interior to itself and thus to further increases in the remanent dipole moment. The total dipole moment saturates, and lies well below the observed value even if Ganymede is allowed to tidally evolve from an orbital position much closer to Jupiter (where the jovian magnetic field is much more intense). Thus Crary and Bagenal (1998) reject Jupiter as the source of a remanent field for Ganymede. They point out, however, that a dynamo field generated in a metallic core in the geologic past could have imposed the requisite remanent magnetization on a cooling external (and sufficiently magnetically susceptible) rock mantle, as long as the paleofield strength was at least 15 times the present value. The requirements on magnetic susceptibility and paleofield strength are more severe if reversals are allowed for (Crary and Bagenal 1998). For essentially similar reasons, Schubert *et al.* (1986) concluded earlier that Ganymede's magnetic field is generated by dynamo action in a liquid or partially liquid metallic core. From a structural point of view, though, the important conclusion is that whether the present field has a dynamo or remanent origin, a metallic core is required.

The internal structure of Ganymede is constrained by the satellite's density and moment of inertia, but these data by themselves cannot be inverted to a unique configuration. With inferences from the magnetometer measurements and cosmochemistry, however, the range of possible interior structures can be bounded. For example, we can assume that Ganymede is fully differentiated into an ice shell, a rock mantle, and a metallic core. Figure 13.4 from Anderson *et al.* (1996a) shows contours of rock mantle radius (in fractions of R_G) as a function of core mass (as a fraction of M_G) or core radius (as a fraction of R_G) and ice shell density, for two plausible metallic core densities and a rock mantle density similar to that of the Earth's upper mantle (all layers are uniform). Contours of the allowable C_{22} and moment-of-inertia range are over-plotted. Formally, these models indicate a broad range in possible core size between ≈ 0.15–$0.2R_G$ and 0.4–$0.5R_G$. In practice, the range is narrower: the upper bounds correspond to little silicate mantle (cosmochemically implausible), while the lower bounds correspond to implausible ice shell densities (given that higher density polymorphs dominate). The smallest cores are also so small that they call the energetics of the dynamo into question (dipole fields fall off as $1/r^3$).

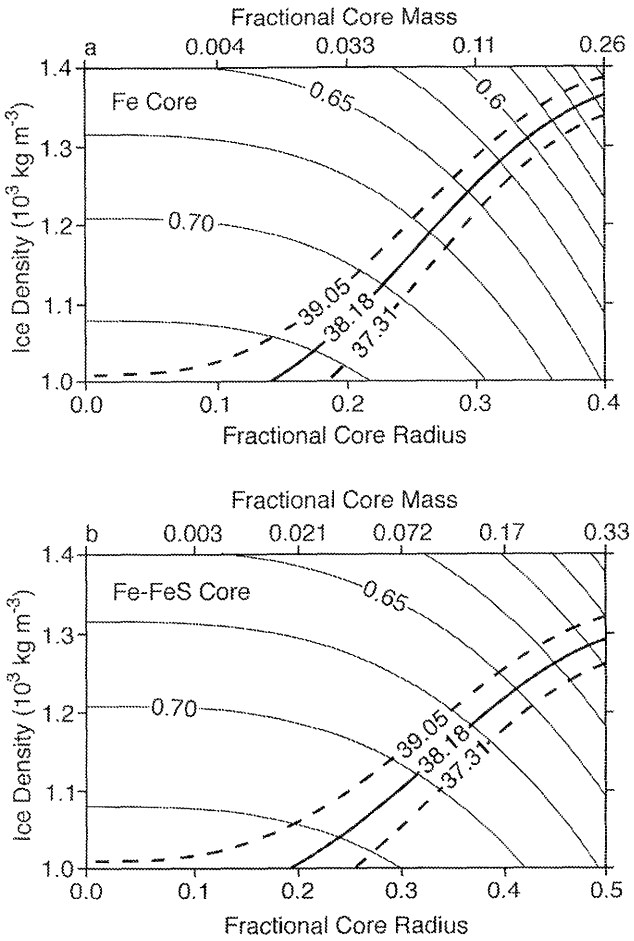

Figure 13.4. Representative Ganymede three-layer models having a rock mantle density of 3300 kg m^{-3} are shown for (a) a pure Fe core (density 8000 kg m^{-3}) and (b) an Fe–FeS core (density 5150 kg m^{-3}). Rock mantle radii are contoured as a function of metallic core size and ice shell density, but only those models that fall near the solid curve labeled $38.18 \pm 0.87(\times 10^{-6})$ have the proper C_{22} and moment of inertia. Adapted from Anderson *et al.* (1996a).

More sophisticated structural models have been calculated by Kuskov and Kronrod (2001a), Sohl *et al.* (2002), and McKinnon and Desai (2003). Figure 13.5 illustrates a suite of models from Sohl *et al.* (2002). The models take into account the temperature and pressure effects on a water-ice shell overlying an olivine mantle surrounding metallic cores of varying compositions between Fe and FeS. The models assume a solid state equation-of-state for the Fe–FeS core, a common approach though Ganymede's core must at least be partially molten to account for the dynamo. A pure olivine mantle is also an approximation to a more complex rock mineralogy, but it is a legitimate one (e.g., olivine is the dominant mineral in the Earth's upper mantle). Figure 13.5 therefore gives a reasonable indication of the bounds on Ganymede's gross internal structure. Core sizes are expected to lie between 650 and 900 km radius and the ice shell should be about 900 km thick.

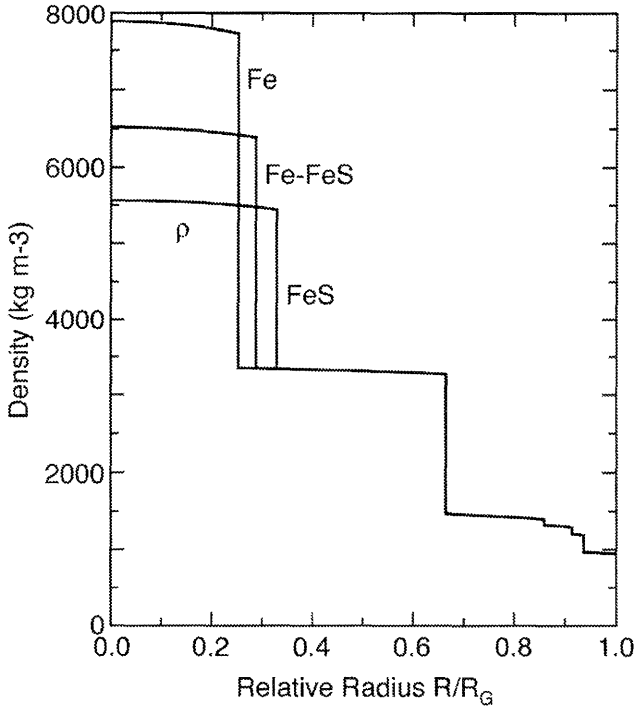

Figure 13.5. Radial distribution of Ganymede's density for three hypothetical core compositions of Ganymede. The models satisfy the mean density and moment-of-inertia constraints. Adapted from Sohl *et al.* (2002).

Kuskov and Kronrod (2001a) based 3-layer mantle mineralogies on a variety of ordinary and carbonaceous chondrites, and used a realistic ice equation of state for the outer shell and constant densities for the cores (the same two densities as in Anderson *et al.* 1996a). Geophysically admissible models (in the sense of satisfying the density and moment-of-inertia constraints) were evaluated in terms of bulk Fe/Si and mass fraction of iron in the core (Fe metal and FeS versus total Fe). If these ratios were deemed to be self-consistent, in that they were similar to the chosen meteoritic model, then that meteorite was accepted as a possible model for Ganymede's bulk composition. For the most reasonable of their two ice shell models (the one that is not partially molten to its base), the best match is given by L chondrites (possibly LL chondrites), and the core is Fe rich. While there is no logical genetic link between a reduced, volatile-depleted, iron-metal-bearing meteorite class from the inner asteroid belt and a very volatile-rich major body formed around Jupiter, the inference from these models is that "Ganymede-rock", like the L and LL chondrites, may be depleted in iron with respect to solar values.

Sohl *et al.* (2002) calculated suites of geophysically admissible 3-layer Ganymede models (ice shell/rock mantle/metallic core) with constant densities for each layer (these are simpler models than those in Figure 13.5). Interpreting the range in mantle densities as a variation in iron content of the single mineral, olivine, they find a broad range of total (mantle + core) Fe/Si ratios above solar. While it is clear that supersolar Fe/Si ratios, if they had been found, would have been rejected by Kuskov and Kronrod (2001a) as not resembling any known chondrite, it is not obvious why some geophysically admissible subsolar Fe/Si models were not uncovered by Sohl *et al.* (2002). One possibility is the mantle stoichiometry assumed by Sohl *et al.* (2002). Had they used a mix of olivine + pyroxene + garnet their range of Fe/Si values might have been different.

McKinnon and Desai (2003) elaborate on the Ganymede modeling in Mueller and McKinnon (1988) by incorporating liquid Fe–S–O cores. Their approach bases mantle and core compositions on solar proportions of Fe, Mg, Ca, Al, and S to Si, with realistic equations-of-state and temperature profiles for all layers. The closest meteoritic analogue for the rock + metal in these models is a dehydrated carbonaceous chondrite (ordinary chondrites are too sulfur depleted). McKinnon and Desai (2003) find that fully differentiated models of Ganymede with solar composition mantles and cores do not simultaneously satisfy the density and moment-of-inertia constraints. If the density is matched, then the moment of inertia falls short ($\approx$0.300–0.306 *vs.* 0.3115, depending on the oxidation state of the mantle and core). One explanation is that Ganymede's Fe/Si ratio is indeed subsolar, which implies a larger mantle + core and total moment of inertia, and thus supports the conclusions of Kuskov and Kronrod (2001a). This explanation is non-unique, however. Alternatively, there may be a small non-hydrostatic contribution from the rock mantle to the second-degree gravity field. This would cause the Radau–Darwin relationship to overestimate the moment of inertia. Such contributions are measurable for all the terrestrial planets, and McKinnon and Desai (2003) show that if only a fraction ($\sim$20%) of the smallest observed non-hydrostatic component is scaled to Ganymede conditions, then a solar-composition mantle + core could yield a C_{22} and J_2 that agree, within the 1-σ error, with Anderson *et al.* (1996a).

In summary, the gross features of Ganymede's structure appear set, but refinement of the structure and the choice of compositional alternatives will require more data. Barring direct structural information, such as from seismology, the most telling would be the measurement and analysis of a more complete gravity field (e.g., Anderson *et al.* 2001a, and our earlier discussion).

13.5.1 Thermal Evolution and Core Formation

Three major issues present themselves with respect to Ganymede's thermal history: (1) separation of rock + metal from ice; (2) separation of metal from rock; and (3) origin of the magnetic field. We discuss each in turn.

Regarding the primary differentiation of Ganymede – the separation of its denser rock and metal phases from its ices – it was recognized early on that there was more than enough accretional energy to melt its ice fraction, and substantially so (e.g., Schubert *et al.* 1981). In order for a Ganymede-like satellite to be minimally or only modestly differentiated, as Callisto appears to be (Anderson *et al.* 1998a, 2001c, and below), the accreting objects should not be so large as to deeply bury their heat and the accretion time should be long enough that accretional energy can be efficiently radiated to space from the surface (McKinnon and Parmentier 1986). The latter requirement has always been difficult to understand in traditional models of satellite formation in a sub-jovian nebula, given the very short

dynamical timescales involved (Stevenson *et al.* 1986, see Section 13.8 for a fuller discussion).

The gas-starved-disk model of Canup and Ward (2002) solves the timescale problem for Callisto, in that satellite accretion persists as long as the solar nebula exists after Jupiter formation. It may solve the problem too well, however, because it is not obvious that a deeply differentiated Ganymede is also predicted. The alternative model of Mosqueira and Estrada (2003a,b) argues that Io, Europa, and Ganymede form in what resembles a traditional jovian subnebula (i.e., rapidly), whereas more distant Callisto forms in a different, and slower dynamical regime (see Section 13.8). A deeply melted Ganymede is predicted in such a scenario (Lunine and Stevenson 1982, Kirk and Stevenson 1987), but its orbital stability in the subnebula remains a question (Stevenson *et al.* 1986, Canup and Ward 2002).

A modestly differentiated Ganymede may nevertheless have evolved to be deeply differentiated. If the Laplace resonance formed by means of differential orbital expansion, Io, Europa, and Ganymede may have been temporarily captured into other Laplace-like resonances before reaching their final resonant configuration (Malhotra 1991). Ganymede's orbital eccentricity would have been excited while in temporary resonance, and the satellite could have been substantially tidally heated (Malhotra 1991, Showman and Malhotra 1997, Showman *et al.* 1997). The magnitude of this heating could have driven separation of ice from rock+metal deep in Ganymede, via ice melting, especially since the differentiation may have been self-sustaining due to the release of gravitational potential energy as differentiation proceeded (Friedson and Stevenson 1983, Mueller and McKinnon 1988). For tidal heating to be effective, the rheology of the rock–ice layer must be sufficiently weak. This may be a problem if the rock dominates the rheology and the temperature is below the ice melting temperature. The existence of this tidal heating episode is uncertain; in the model of Peale and Lee (2002), the Laplace resonance is primordial. In this case the deep differentiation of Ganymede, starting from a state of modest differentiation, and not of Callisto, requires that the modest advantages Ganymede has over Callisto in this regard (slightly greater rock fraction, slightly greater radiogenic heating and ice–rock viscosity due to the greater rock fraction, and greater specific gravitational potential energy) combine tellingly (Friedson and Stevenson 1983, McKinnon and Parmentier 1986, Mueller and McKinnon 1988). The Peale and Lee (2002) scenario does not explain the roughly 50% resurfacing of Ganymede that occurred some time after the satellite formed. The relatively lightly cratered areas may be only about 2 Gyr old, though there is a large uncertainty in the absolute ages (Zahnle *et al.* 2003). The late transient capture into a Laplace resonance provides an explanation for this late deformation event. This is clearly an area in which new modeling is needed.

Once a rock+metal interior body, or "primordial core" forms, and we stress that the geophysical evidence that most or all of Ganymede's rock+metal lies in a core is secure, the question turns to the existence and dynamics of further differentiation into a metallic core and overlying rock mantle. McKinnon (1996) showed that radiogenic heating alone was sufficient to bring the interior of a mixed rock+metal primordial core to the melting temperature of a sulfur-bearing

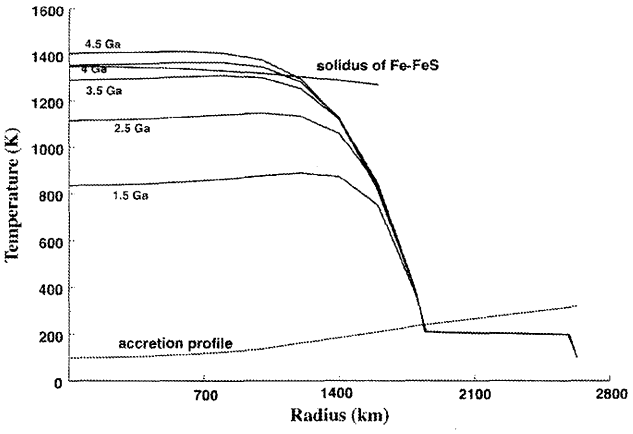

Figure 13.6. Temperature as a function of depth and time during warming of the interior of Ganymede by the decay of radioactive elements with an initial heat production rate of 30 pW kg^{-1}. Also shown is the solidus (eutectic) of Fe–FeS (Boehler 1996). The solidus is reached after 3.6 Gyr in this model. The timing is controlled by both the initial (accretional) temperature profile and the heat production rate. Adapted from Spohn and Breuer (1998).

metallic phase (cf. Kirk and Stevenson 1987). A chondritic mixture of non-ice elements contains sufficient U, Th, and ^{40}K to cause a temperature rise of ~100 K per 100 Myr if there is no heat loss. The interior of a body the size of Ganymede's primordial core is conductively isolated from the exterior ice for very long times, so the internal temperatures should rise essentially unchecked to levels appropriate to solid state convection (see Figure 20 in the chapter by Greeley *et al.* for a similar calculation for Europa). Before that occurs, however, the Fe–FeS eutectic (lowest melting point) temperature (or that in the FeO–FeS system if the interior is sufficiently oxidized, Naldrett 1969) is reached. The Fe–FeS eutectic temperature is ~1265 K at low pressure, and falls to ~1190 K at 10 GPa (Fei *et al.* 1997), the approximate central pressure in Ganymede today. Once a sufficient melt fraction accumulates, the excess can drain downwards under the action of gravity to form a core (e.g., Yoshino *et al.* 2003). It can further be shown for Ganymede that the energy consumed by the latent heat of melting of the metal is more or less balanced by the gravitational potential energy released by core formation. This process was also modeled by Spohn and Breuer (1998). Figure 13.6 shows how the rock+iron core in the model of Spohn and Breuer (1998) heats up due to radioactive decay to reach the Fe–FeS solidus (eutectic).

The composition and size of the core depends on the composition of the Fe-bearing phases that melt to form it and the completeness of that melting. A CI chondritic Fe–FeS composition is 23 wt% S (Lodders and Fegley 1998), and while on the Fe side of the eutectic at low pressures, it ends up on the FeS side at pressures deep within Ganymede (i.e., the eutectic composition is pressure sensitive, Fei *et al.* 1997). Moreover, if the interior of Ganymede is sufficiently oxidized, the composition may approach that of FeS (e.g., Scott *et al.* 2002), while still greater degrees of oxidation stabilize magnetite as a potential core phase (unfortunately, the

melting relations in the Fe_3O_4–FeS system are very poorly known at high pressure). Oxidation at an earlier stage in Ganymede's evolution may also have released S and SO_2 (as argued for Io by Lewis 1982) to the ice layer, and so offers a route to reduce the amount of sulfur in the core. Thus, a range of processes exist that may modify even an initially chondritic composition, but the core that forms should certainly be FeS rich. Specifically, though, a chondritic, metallic Fe–FeS mixture is likely to be completely melted (or nearly so) at interior temperatures controlled by silicate convection early in Ganymede's history, and a thermal excursion due to tidal heating (Showman and Malhotra 1997, Showman *et al.* 1997) makes this conclusion more secure.

Once formed, the evolution of the core is determined by the heat released within and transferred through the overlying rock mantle. By the present era, and without tidal heating, Ganymede's mantle might be conductive throughout and cooling, but core temperatures are very unlikely to have dropped below the Fe–FeS eutectic temperature (McKinnon 1996). Thus the core of Ganymede today should be at least partially molten, which satisfies one prerequisite for a magnetic dynamo (Schubert *et al.* 1996). A more stringent prerequisite for a dynamo, however, is that the mantle is presently cooling the core at a rate sufficient to maintain convective motions in the core. At a minimum, the mantle must be able to accommodate the heat flow conducted down the core adiabat. Estimates of the magnitude of this heat flow are uncertain, but this constraint on dynamo action in Ganymede's core may require the mantle to be convective at present.

The core convective motions maintaining Ganymede's magnetic dynamo are powered by either thermal or compositional buoyancy, or both. In the case of the Earth, compositional buoyancy is provided by the freezing of an Fe–Ni inner core that concentrates the light element into the outer core (e.g., Stevenson *et al.* 1983). The Earth's dynamo is driven by a combination of core cooling, the latent heat released by inner core solidification, and the gravitational energy released by the differentiation accompanying inner core solidification (Stevenson *et al.* 1983, Buffett *et al.* 1996). It is even possible that radioactivity in the Earth's core drives outer core convection and the dynamo (Gessmann and Wood 2002, Rama Murthy *et al.* 2003). Kuang and Stevenson (1996) argue that cooling and freezing of Ganymede's core (without tidal heating input) will not provide sufficient thermal energy for convection and dynamo action in the liquid portion of Ganymede's core, and so favor compositional convection as the driving mechanism. If the core sulfur content is under $\sim$21 wt%, an iron inner core should form, as on the Earth (and equivalently, an Fe_3O_4 inner core should form if the core is sufficiently oxygen rich). Compositional buoyancy is problematic for cores that are close to FeS in composition, however. While an inner core of solid FeS should readily form due to freezing under pressure (Boehler 2000), it would release a denser, more Fe-rich liquid, suppressing convection. More exotic possibilities also exist such as the "raining up" of FeS crystals for appropriate compositions (McKinnon 1996), and tidal heating during formation of the Laplace resonance may have enhanced or restarted core convection as well (Stevenson 1996b, Schubert *et al.* 1996). These are intriguing ideas, but no quantitative model of Ganymede's dynamo has been published (but see Sarson *et al.* 1997). Satellite dynamos remain a fascinating, unsolved problem in planetary geophysics.

13.6 CALLISTO – INTERIOR MODELS

Callisto is similar in size and density to Ganymede, but its relatively dark, heavily cratered surface early on suggested that it was undifferentiated (Schubert *et al.* 1981, 1986). McKinnon and Parmentier (1986) argued that Callisto's appearance was deceiving, its subsurface might be ice rich, and that it might have undergone an earlier evolution similar to that of Ganymede. *Galileo* imagery has been decisive in that no traces of such ancient geologic activity are seen (Chapter by Moore *et al.*), but notably, Callisto appears to be partially differentiated after all (Anderson *et al.* 1998a, 2001c). Even more remarkably, it appears to possess an internal ocean (e.g., Zimmer *et al.* 2000, Chapter by Kivelson *et al.*). Callisto does not have an internal magnetic field (Khurana *et al.* 1997b, Chapter by Kivelson *et al.*), consistent with its partially differentiated state and its lack of a metallic core.

Callisto's mean density is 1834.4 ± 3.4 kg m^{-3}, its mean radius is 2410.3 ± 1.5 km (Table 13.1) and its gravitational coefficient C_{22} is $10.2 \pm 0.3 \times 10^{-6}$ (Table 13.2). All of the *Galileo* flybys of Callisto were equatorial, so there is no independent constraint on J_2 or whether slowly rotating Callisto is in a hydrostatic state; the fit to $S_{22} = -1.1 \pm 0.3 \times 10^{-6}$ is non-zero to 3σ (Anderson *et al.* 2001c), suggesting that our understanding of Callisto's gravity field is incomplete (i.e., S_{22} should be zero in hydrostatic equilibrium in the tidal axis coordinate system). Nevertheless, a hydrostatic Callisto is reasonable, and can be justified *a posteriori* in that much or all of Callisto's internal structure may be controlled by the creep and yield strength of (relatively weak) water ice (Anderson *et al.* 2001c, and above).

Assuming that Callisto is hydrostatic, the value of C_{22} above yields a normalized moment of inertia $C/MR^2 = 0.3549 \pm 0.0042$ (Table 13.1). This moment-of-inertia value, while clearly larger than that of Ganymede, is significantly lower than that of a completely undifferentiated Callisto (McKinnon 1997, $C/MR^2 \approx 0.38$). The rock+metal fraction in Callisto must increase with depth, but gravity data alone are unable to constrain the exact nature of this increase (i.e., whether it is continuous or step-wise). A continuous increase is ruled out, because it would suppress internal convection by solid state creep of the ice fraction, and the resulting conductive temperature gradient would intersect the melting curve and promote further differentiation. Callisto, then, must be layered in terms of its ice/rock ratio (except perhaps for small, restricted regions).

The simplest layered model for Callisto consists of a denser (more rock and dense-ice-phase rich) interior surrounded by a less rock-rich and more low-density-ice-polymorph-rich shell. Figure 13.7 contours the thickness of such an outer shell in terms of the densities of the two layers. Contours delineating models consistent with the inferred moment of inertia (C_{22} values) are included in the figure. A broad range of shell thicknesses is shown. The interior density is, however, almost certainly limited to that of a cool, undifferentiated and dehydrated rock+metal sphere ($\leq$3850 kg m^{-3}), so the upper limit on shell size is

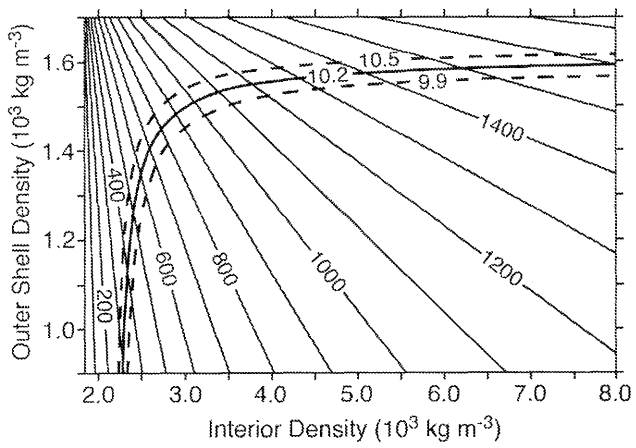

Figure 13.7. Callisto two-layer model. Ice-rich outer shell size is contoured as a function of outer shell density and ice-poor interior density. Only those models that fall near the solid curve labeled $10.2(\pm 0.3) \times 10^{-6}$ have the proper C_{22} and moment of inertia. From Anderson *et al.* (2001c).

~1250 km. The lower limit on the thickness of a clean ice outer shell, with or without an ocean, is ~300 km.

The rationale for two-layer models is that rock(+metal) can separate from ice if the ice melts or if the rock is in massive enough fragments (or concentrations) that they sink slowly through the ice. The downward Stokes velocity of the rock fragments must exceed interior convective velocities for the latter separation to be effective (Schubert *et al.* 1981), but not be so great that the rock escapes remixing with deeper ice–rock, if the two-layered structure is to be maintained. Rock released by melting need not sink with respect to the ice, as long as water can escape to higher levels, but the rock must also remix with deeper ice–rock if the two-layered structure is to be maintained.

Whether descending rock fragments (or concentrations) remix with deeper ice–rock depends on the fragment or concentration size and ice viscosity, which are unknown. If, however, the rock descends to the center of Callisto, then a rock core should form, surrounded by a mixed ice–rock layer and an exterior ice shell. Such 3-layer models were explored in detail in Mueller and McKinnon (1988). Their calculations, in which the mixed layer has the same ice/rock ratio as the bulk satellite, indicate that Callisto could be a body with $18 \pm 4\%$ of its total rock in a central core ~900 km in radius. New models indicate that under such conditions the boundary between the clean ice and mixed ice–rock layer is very close to the depth of ice I–ice III transition pressure (207 MPa) (McKinnon and Desai 2003). This depth is also the natural level for an ocean (Zimmer *et al.* 2000, and see discussion below), so it is tempting to imagine that thermal conditions that led to melting within Callisto operated at the ice minimum-melting temperature, and that the separated rock+metal was able to descend to form a core. However, unless our hydrostatic interpretation of the second-degree gravity field is in error, Callisto is not deeply differentiated. The runaway ice melting and differentiation of Friedson and Stevenson (1983), if it began, stalled; similarly, the boundary layer melting possible in the hotter convecting, mixed ice–rock shell (Mueller and McKinnon 1988), if it occurred, did not lead to deep differentiation either. Runaway differentiation is favored energetically, but its dynamics must initially be slow enough that Callisto remained cool and largely unmelted if this structural interpretation is to make sense.

If, on the other hand, the interior rock and ice remains mixed during differentiation, then the clean ice layer necessary to account for the mass and moment of inertia of Callisto must be thicker (~300 km, Anderson *et al.* 2001c). This could arise if accretional melting was this deep or extensive, or if a zone of partial melting and refinement (rock from ice) (Friedson and Stevenson 1983) extended to 300 km depth (~0.4 GPa). Given the amount of gravitational potential energy that can be released during differentiation (Friedson and Stevenson 1983), Anderson *et al.* (1998a, 2001c) argue that partial differentiation by melting would release sufficient heat to drive further differentiation, and that a thermal runaway would ensue. They therefore argue that the differentiation process on Callisto occurred (and is occurring) by slow, solid-state separation of rock from ice. Nagel *et al.* (2003) present a possible model of this process in which ice–rock separation does not involve the ocean. In fact, Nagel *et al.* (2003) argue that the ocean forms relatively late, after the near-surface ice layer has been mostly cleared of rock and the ice minimum-melting pressure has migrated to a deeper, sufficiently warm level (see next section).

13.7 THERMAL CONSIDERATIONS IN THE MAINTENANCE OF INTRA-ICE OCEANS ON THE ICY GALILEAN SATELLITES

As discussed in the preceding sections, subsurface liquid water oceans are likely on all three icy Galilean satellites. The evidence is based on *Galileo* magnetometer observations of electromagnetic induction in these satellites; the signature is seen most clearly at Callisto (Khurana *et al.* 1998, Neubauer 1998, Kivelson *et al.* 1999, 2000, 2002b). The magnetic field data allow estimates of the thickness of the ice layers covering the oceans (e.g., Zimmer *et al.* 2000). For Europa, the strength of the induced signal is consistent with an ocean underneath a thin ice shell a few tens of kilometers thick. For Ganymede and Callisto the oceans are probably at greater depths of 200 km or more. The existence of an ocean underneath tens of kilometers of ice on Europa is supported by geological evidence (Pappalardo *et al.* 1999). Other evidence favors even thinner ice layers (e.g., Greenberg *et al.* 1998). Similar geologic evidence for oceans is not available for Ganymede and Callisto, although it has recently been argued that the lack of hilly and lineated terrain antipodal to major impact basins on Callisto may suggest an ocean that would have damped the seismic waves generated by the impact (Williams *et al.* 2001). At least for Callisto, the inferred existence of an ocean is surprising since this satellite is incompletely differentiated (Anderson *et al.* 2001c, Sohl *et al.* 2002) and devoid of endogenic activity (as witnessed by its old surface).

Hussmann *et al.* (2002) have shown that tidal heating in an europan ice shell a few tens of kilometers thick can keep a subsurface ocean from freezing. Moreover, Spohn and Schubert (2003) have demonstrated that a subsurface liquid water ocean on Europa is likely even with internal heating limited to what is generated by radioactive decay in the

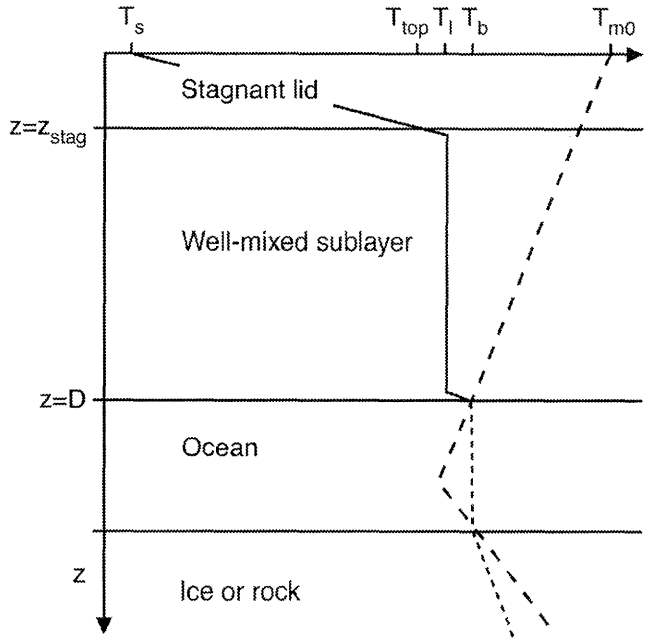

Figure 13.8. Water-ice phase diagram and thermal model of the outer layers of an icy Galilean satellite with a convecting ice shell. The top layer is the stagnant lid. Below the stagnant lid is the well mixed sub-layer through which heat is transferred by convection. The case for a conductive shell is equivalent to a stagnant lid extending all the way to the bottom of the shell. The temperature profile in the ice shell is shown with solid lines. The melting temperature is shown with dashed lines and the temperature profile in the ocean and the ice layer below the ocean is shown with dotted lines. On the top and bottom of the well-mixed layer there are thermal boundary layers with large temperature gradients.

rocky part of the satellite. Radiogenic heating in the rocks of Ganymede and Callisto could be adequate for the maintenance of liquid water oceans deep in their interiors, but the case for these satellites is not as strong as the one for Europa (Spohn and Schubert 2003), as will be discussed below.

13.7.1 Melting Relations

Subsurface oceans on satellites are possible because of the anomalous melting behavior of ice I for which the melting temperature decreases with pressure until it joins the ice I/ice III transition and the ice III melting curve in a triple point at a pressure of 207 MPa and a temperature of 251.15 K (Chizov 1993). A sketch of the ice melting temperature as a function of depth together with a simple thermal model of the outer shells of an icy satellite is shown in Figure 13.8. The triple point pressure translates into different depths for the three satellites because of their differing masses and, possibly, ice shell densities. Assuming an ice shell density of 1000 kg m^{-3}, a depth of 160 km is obtained for Europa, about as deep as the total thickness of the water layer, which is believed to be around 150 km (Anderson *et al.* 1997, 1998b, Sohl *et al.* 2002). The depth of the minimum melting temperature is about 145 km in Ganymede if an ice shell density of 1000 kg m^{-3} is assumed. This density is reasonable since Ganymede is most likely differentiated (Anderson *et al.* 1996a, 2001a). For Callisto, the ice shell density could be about 1600 kg m^{-3} if the satellite has a mostly undifferentiated, cold and stiff outer shell (presuming such a shell is geologically stable). This density is calculated from the density of ice I, a concentration of rock of about 50 weight-percent, and a rock density of 3500 kg m^{-3}. With this ice shell density, the triple point in Callisto would occur at a depth of about 100 km. If the density in the ice shell were 1000 kg m^{-3}, the depth to the triple point would be about 165 km.

It is possible that the melting point is even further depressed if the ice in the satellites is not pure H_2O but contains other components such as ammonia, methanol and/or salts (e.g., Kargel 1992). The evidence for induced magnetic fields from electric currents in the oceans requires an electrolyte such as salt. Pure water oceans can therefore serve as an extreme case only. Because the melting point depression is smallest for pure water ice, water oceans are the least likely to occur. If a water ocean is found to be possible, then a salty ocean will be even more likely. The phase diagram of the water–ammonia system is reasonably well studied (Hogenboom *et al.* 1997, Sotin *et al.* 1998) and can serve as a model. Ammonia hydrates are predicted condensates in the satellites of Jupiter as long as temperatures in the sub-jovian nebula are cool enough and thermochemical equilibrium is achieved (Prinn and Fegley 1981, 1989). This is probably most applicable to Callisto and possibly Ganymede (see Section 13.6). The concept of internal layers of ammonia–water liquid is well developed in the literature (Kargel 1998, Sotin *et al.* 1998). The water–ammonia liquidus temperature depends on pressure and on the concentration of ammonia in the water.

The evolution of an ice lid and ocean will depend not only on the bulk concentration of ammonia but also on the initial conditions. If the lid grew on top of an ocean with some initial concentration of ammonia and starting from zero thickness, then the lid will be pure water ice. The composition of the ocean will be determined by the mass of the water ice removed from the ocean and the constancy of the ammonia mass. The lid bottom temperature will be determined by the liquidus surface, the composition of the ocean, and the pressure at the bottom of the lid. Grasset and Sotin (1996) have suggested a possible path on the liquidus surface starting from a low NH_3 concentration and continuing to the high pressure eutectic at 29 wt-% NH_3, 170 MPa and 176 K. The pressure of 170 MPa is equivalent to a depth of about 130 km on Europa, 120 km on Ganymede, 80 km on Callisto if the outer shell is an undifferentiated ice–rock mixture and 135 km if the outer shell is mostly ice.

If the satellite were initially at subsolidus temperatures and was warmed to reach the ammonia hydrate solidus (eutectic), melt would form at a temperature of 176 K and mostly independent of pressure. The composition of the melt under these circumstances would be around 30 weight-% ammonia, decreasing slightly with pressure, because the composition along the eutectic/peritectic is almost constant. Since the ice is less dense than the fluid, the ice will tend to float on top of the forming ocean. The rate at which the ice will separate and float will depend on the rheology and the concentration of the melt in the solid. As the temperature increases, water will dilute the melt, further the formation of an ocean by gravitationally separating the ice from the melt, and the composition of the ocean and the temperature at the base of the lid will be determined by the pressure at

the base of the lid, the bulk concentration of ammonia, and the liquidus surface.

13.7.2 Energy Balances and Equilibrium Models

For Europa, it is possible to attribute the existence of an ocean to tidal heating. This is not possible for Ganymede and Callisto; tidal heating is negligible at their present orbital distances and eccentricities. On these satellites, oceans must be due to radiogenic heating or to heat buried at depth and released through satellite cooling. It has been speculated (Malhotra 1991, Showman and Malhotra 1997, Showman *et al.* 1997) that Ganymede went through a phase of intense tidal heating perhaps as little as 1 Gyr ago when it passed into the present resonance through a 3:2 resonance. During such a transition, the eccentricity would have increased by as much as a factor of 10 which could have caused runaway melting of ice and the formation of an ocean if the ice layer was warmer than 200 K. For colder initial temperatures, runaway tidal heating and melting is avoided because the ice rheology is too stiff and the tidal deformation is too small. A simple assessment of the feasibility of an ocean can be made if one assumes that the outer shell is conductive and that the melting curve is linear. For pure ice, the surface melting temperature T_{m_0} is 276.1 K and the slope of the melting dT_m/dp curve from $p = 0$ Pa to the triple point is -1.063×10^{-7} K Pa^{-1}. This converts to values of -0.138 K km^{-1} for Europa, -0.168 K km^{-1} for Ganymede, and -0.213 K km^{-1} for an undifferentiated outer Callisto shell (-0.133 K km^{-1} for a pure ice outer Callisto). For 5 weight-% ammonia and the melting curve proposed by Grasset and Sotin (1996) introduced above, the values are $T_{m_0} = 266.9$ K and $dT_m/dp = -5.647 \times 10^{-7}$ K Pa^{-1}. The latter converts to: -0.734 K km^{-1} for Europa, -0.892 K km^{-1} for Ganymede, and -1.13 K km^{-1} for an undifferentiated outer Callisto shell (-0.706 K km^{-1} for a pure ice outer Callisto shell). The thickness of the shell D that is in equilibrium with an assumed heat flow into the base of the ocean can then be calculated to be approximately (Spohn and Schubert 2003)

$$D = \frac{T_{m_0} - T_s}{\frac{q}{k} - \frac{dT_m}{dz}} \tag{13.20}$$

where T_s is the surface temperature and q is the heat flow evaluated at the surface. The present surface temperatures are 105 K for Europa, 120 K for Ganymede and 130 K for Callisto. The bottom heat flow can be scaled by the heat flow in equilibrium with the present chondritic radiogenic heating rate of 4.5 pW kg^{-1}. This heating rate will result in equilibrium surface heat flows of 5.6 mW m^{-2} for Europa, 3.9 mW m^{-2} for Ganymede, and 3.4 mW m^{-2} for Callisto. At the depth of the triple point, the equilibrium heat flows are 7.0 mW m^{-2} for Europa, 4.3 mW m^{-2} for Ganymede, and 3.6 mW m^{-2} for Callisto. A representative value for the thermal conductivity of the ice is 3.3 W m^{-1}K^{-1}.

An ocean is likely if D is found to be smaller than the depth to the triple point pressure or to the pressure at the eutectic. The following shell thicknesses are obtained: For pure ice, no ammonia, we find about 91 km for Europa, 116 km for Ganymede, 108 km for an undifferentiated ice–rock shell on Callisto and 125 km for a pure ice shell on the same satellite (cf. Ruiz 2001). With the exception of the rock–ice shell, these are all notably smaller than the depths to the triple point suggesting the likelihood of oceans. For 5 weight-% ammonia the case for an ocean is even stronger, as is expected. Here the lid thicknesses are 65 km for Europa, 77 km for Ganymede, 83 km for an undifferentiated ice–rock shell on Callisto and 66 km for a pure ice shell on the same satellite.

For simplicity, we have assumed that the shells are purely conductive. It is possible that a shell could become thick enough to be unstable to convection, in which case the shell would grow to a greater thickness than calculated here. The stability is mostly a function of temperature and rheology, but it also depends on the heat flow from below and the thermal conductivity. Spohn and Schubert (2003) have explored a wide range of models to investigate the possibility of present oceans in the Galilean satellites as a consequence of an assumed heat flow from below the ocean. Both conductive and convective heat transfer mechanisms in the ice lithosphere were considered depending on the stability of the layer to convective overturn. Convection, if it occurred, was assumed to be in the stagnant lid regime (Solomatov 1995, Grasset and Parmentier 1998) and the viscosity of the ice was assumed to be given by

$$\nu = \nu_0 \exp A \left(\frac{T_m}{T} - 1 \right) \tag{13.21}$$

with T_m the depth-dependent melting temperature and representative values of $A = 24$ and $\nu_0 = 10^{14}$ Pa s (a simplified but commonly used rheological model, cf. Durham and Stern 2001). For the same parameter values, the conclusions from the more complete models of Spohn and Schubert (2003) differ from the estimates presented above only for the no ammonia, pure ice models. In these cases, convection may become important, and, depending on uncertain parameter values that relate convective vigor to heat flow, convection might freeze the oceans. This is more likely to happen for Ganymede and Callisto than for Europa, but the oceans will in any case then be only a few kilometers thick.

13.7.3 The Probability of Oceans and their Thicknesses

The thickness estimates presented above and the much more extensive results of equilibrium models presented by Spohn and Schubert (2003) are clear-cut for water+ammonia. Oceans are predicted for all three satellites and the conclusion is robust against parameter variations. The water ice shells on top of the H_2O–NH_3 oceans are similar in thickness (70–90 km). The thickness of these oceans is substantial. For Europa, the ocean thickness is limited by the thickness of the water shell (about 150 km) leaving only about 80 km for the ocean. This limitation does not apply to Ganymede and Callisto whose bulk densities and moments of inertia indicate a thick ice shell (e.g., Anderson *et al.* 2001a,c, Sohl *et al.* 2002). The thickness of the H_2O–NH_3 oceans may well be 200 to 300 km. For Callisto this would allow a structure of an ice shell with or without rock in it overlying an ocean that could extend close to the surface of a possible ice–rock core. The ice shells would be thinner and the oceans even thicker if the bulk concentration of ammonia were greater than assumed in our model. Unfortunately, we have no in-

dependent evidence for or constraint on the concentration of ammonia in the Galilean satellites.

The case for oceans in the icy satellites of Jupiter is less clear if the ice is pure or if the melting point depression is small. In these cases the differences among the satellites will matter, as well as choices of uncertain parameter values. The likelihood of an ocean increases with decreasing pressure gradient ρg in a satellite and with increasing heat flow per unit area. This is why Europa, which has the greatest heat flow per unit area and the smallest pressure gradient of 1.3 kPa m^{-1} of the three satellites, is the most likely to have an ocean under these circumstances. The pressure gradients in Ganymede and Callisto are about 1.6 kPa m^{-1} and 2 kPa m^{-1}, respectively. The likelihood of an ocean in Europa will be further strengthened if tidal heating is considered. Hussmann *et al.* (2002) have calculated tidal heating rates in Europa's ice shell and have searched for equilibrium between the tidal heating and heat transfer rates, both of which are functions of the ice shell thickness and the ice rheology. For similar values of the rheology parameters as used in Spohn and Schubert (2003) they find that the equilibrium value of the tidal heating rate, when expressed as a surface heat flow, is about 3 times the heat flow due to radiogenic heating, and the ice shell thickness is 20–40 km.

An undifferentiated Callisto is the most likely satellite not to have an ocean on the basis of these considerations. An ocean is unlikely, mostly because the rapid increase in pressure caused by the assumed outer shell density of 1600 kg m^{-3} moves the triple point to a shallow depth of around 100 km. An ice shell of this thickness will be capable of removing the heat due to present-day radiogenic decay in the deeper interior by thermal conduction. Of course, as already discussed, it is unlikely that Callisto is undifferentiated because its normalized moment of inertia is 0.3549 (Anderson *et al.* 2001c, and Table 13.1), smaller than the value of 0.38 for a homogeneous Callisto with density increases through ice phase transformations (McKinnon 1997). Still, the value of the observed moment of inertia has been calculated under the assumption that Callisto is in hydrostatic equilibrium, which it might not be. In any case, it is possible that the outer shell of Callisto carries some rock if the satellite differentiated gradually by the slow inward motion of the rock component. Since the outer shell is cold and rigid, the separation of rock and ice will be very slow there, but the long-term stability of such a density inversion is an open issue. The effect on the depth to the triple point and the presence of an ocean will be the same as in the case of a completely undifferentiated satellite. Of course, our assumption of a more or less primordial concentration of rock in the outer shell may be too extreme. Any reduction in the rock concentration will make an ocean more likely.

While an ocean is very well possible for Europa but questionable for an undifferentiated Callisto, oceans are conceivable for Ganymede and for a partly differentiated Callisto. Thin oceans can be found even under the most unfavorable conditions of pure H_2O and equilibrium between radiogenic heating and heat flow. The former condition is unfavorable because pure H_2O has the highest melting temperature of the candidate ices. The latter condition is unfavorable because satellite cooling should contribute to the energy balance and increase the heating rate above the values derived from radiogenic heating alone. The most important factor acting against oceans is rock potentially left in the outer ice shell during interior differentiation. Rock increases the pressure gradient and moves the triple point of the phase diagram to shallower and colder depths.

There are ways of increasing the likelihood of a more substantial ocean even if ammonia is not present. Other components, e.g., salts such as $MgSO_4$ and $NaSO_4$ (Kargel *et al.* 1991, Kargel 1998), could reduce the melting temperature. Of these, the effect of $MgSO_4$ on the melting temperature has been studied experimentally in the most detail. The effect of $MgSO_4$ (and by extension, other sulfate salts) on the melting temperature of ice is much smaller than that of ammonia, resulting in a reduction of only several kelvins (Hogenboom *et al.* 1995), but it will act to increase the thickness of an ocean and reduce the thickness of the ice shell. Alkali halides such as NaCl have more substantial melting point depressions. Cosmic abundance arguments (Kargel *et al.* 2000, Zolotov and Shock 2001) indicate that the alkali halides will be dilute for thick (tens of kilometers) oceans on the satellites, but when concentrated by freezing into a thin ocean, they may prevent complete freezing.

Other parameters that may increase the likelihood of an ocean are the thermal conductivity and the heating rate. The nominal value of the thermal conductivity used here and in the models of Spohn and Schubert (2003) may be an overestimate if there are substantial ice regoliths on the satellites. The temperature increase through a regolith a few tens of meters thick could be a few tens of kelvins (Fanale *et al.* 1990). This increase will act similar to a reduction of the melting temperature by approximately the same value, or similar to the effect of salt on the melting temperature. The assumed chondritic heat flow from below could, on the other hand, represent an underestimate of the actual heat flow from the deep interior of the satellites. Thermal history calculations for terrestrial planets and satellites (e.g., Schubert *et al.* 1986) have shown that cooling will contribute substantially to the heat flow from the interior. The ratio between the surface heat flow and the rate of radiogenic heating (if expressed as a heat flow) could be as great as a factor of 2 as for the Earth and the Moon (Schubert *et al.* 2001). The value for the Moon, a body of similar size as the Galilean satellites, has been estimated from the numerical results of Konrad and Spohn (1997) and Spohn *et al.* (2001). If this is applicable to the icy Galilean satellites, then there is no problem explaining oceans on all three satellites, as the calculations of Spohn and Schubert (2003) suggest. However, the above ratio between heat flow and heating rate appears to decrease with increasing convective vigor, as measured by the Rayleigh number. The Rayleigh number for Ganymede and Callisto is large, around 10^{12} (see also McKinnon 1998).

Uncertainties in parameter values that work against oceans can also be listed. For instance, if we overestimated the specific chondritic heating rate of 4.5 pW kg^{-1} and the melting point viscosity of 10^{14} Pa s then a correction will tend to make an ocean less likely.

Previous discussions, as, for example, reviewed by Schubert *et al.* (1986), have predicted that the ice shells of the Galilean satellites would be frozen solid because sub-solidus convection would easily remove the heat generated by radioactive decay in the interior. Progress in the parameterization of planetary heat transfer (e.g., Solomatov 1995, Grasset and Parmentier 1998) has resulted in an improved un-

derstanding of the temperature distribution in a convecting planet with strongly temperature-dependent viscosity. These parameterizations known as stagnant-lid convection, thought to be applicable to one plate planets and satellites (but not to the plate-tectonic planet Earth), remove heat mostly by thickening a stagnant-lid or thermal lithosphere on top of the convecting deep interior. Thermal history calculations for the Moon using two- and three-dimensional convection models with the viscosity depending on the laterally averaged temperature profile show the same characteristics (Spohn *et al.* 2001). The previous parameterizations removed heat mostly from the deep interior. It is the lack of cooling the deep interior that effectively results in temperatures above the melting temperature even when convection applies. The relevance of stagnant-lid convection to the Galilean satellites is, however, not entirely certain. Because of plate tectonics, stagnant-lid convection is not relevant to the Earth. If heat transfer processes like lid delamination or water or soft-ice magmatism occur on the Galilean satellites, stagnant-lid convection will not strictly apply. Such processes are perhaps less likely for Ganymede and Callisto because of their thick ice shells, but they could be relevant for Europa and in the past for Ganymede (Schenk *et al.* 2001a). Europa, however, is the satellite for which an ocean is most likely on the basis of our heat balance considerations.

13.8 FORMATION OF THE GALILEAN SATELLITES

The Galilean satellites, an ordered set of bodies of similar mass in coplanar, prograde orbits, and exhibiting an ice/rock compositional gradient, have long been thought of as a "miniature solar system". Therefore, it is naturally assumed that they formed by condensation and accretion in a gaseous subnebula around Jupiter, in a process grossly similar to the accretion of the planets in the solar nebula (Pollack and Fanale 1982, Stevenson *et al.* 1986, Peale 1999). It has also been recognized that the "nebular hypothesis" as applied to satellite systems has some severe drawbacks. Foremost among these are the cooling and condensation times of a minimum mass subnebula, which are much longer ($\sim 10^6$ yr) than both the accretion times of the condensed solids ($\sim 10^3$ yr for large satellites) and the viscous evolution time of the subnebula ($10^3 \times [10^{-2}/\alpha]$ yr) or gas drag timescale of bodies accreted within it ($\sim 10^3 \times [r/1\ \mathrm{km}]$ yr), where α is the Shakura–Sunyaev parameter for effective disk viscosity (typically 10^{-4}–10^{-2}) and r = satellite radius (Stevenson *et al.* 1986). The minimum mass subnebula refers to a theoretical construct in which satellite masses (which for Jupiter total 2.1×10^{-4} M_J, where M_J is the mass of Jupiter) are augmented by H–He gas to achieve solar composition (for a total of $\sim 2 \times 10^{-2}$ M_J) (e.g., Lunine and Stevenson 1982).

The mismatch of timescales is fundamentally due to the small orbital periods of material circling Jupiter (at the position of the Galilean satellites), which means that the subnebula can partially condense, accrete, and lose early generations of (potentially rock-rich) satellites. Even if large satellites manage to form, satellite–disk torques may cause large semi-major axis drifts or even loss of satellites to Jupiter (Lunine and Stevenson 1982, Ward and Hahn 2000).

However, the Galilean satellites exist, and so must have formed in some sort of subnebula. Two major kinds of subnebulae are usually considered for Jupiter (and Saturn) (Pollack *et al.* 1991): an accretion disk, which forms as solar nebula gas and particles flow through the Roche lobes to feed the growing Jupiter during its runaway accretion phase (Pollack *et al.* 1996, Coradini *et al.* 1989), or a spin-out disk, which forms after runaway accretion terminates and the distended, hot Jupiter cools and shrinks, stranding material in a disk in order to conserve angular momentum (Korycansky *et al.* 1991).

More recently, it has been shown that accretion does not terminate so cleanly; even as Jupiter grows to approach its present mass, it opens a gap in the solar nebula around its orbital position, and this greatly reduces but does not necessarily eliminate inflow of solar nebula material (Bryden *et al.* 1999, Lubow *et al.* 1999). This gives rise to the concept of the gas-starved disk, a thin accretion disk that forms after Jupiter's hydrodynamic collapse and lasts for as long as the solar nebula exists to feed it (Stevenson 2001, Canup and Ward 2002). The lower mass and opacity of this disk allows for cooler temperatures, rapid condensation and accretion of available solids, and much longer gas drag and viscous evolution timescales (Canup and Ward 2002) – timescales compatible with large satellite survival over the lifetime of the subnebula. In this scenario, the satellites grow over a protracted period (possibly $>10^6$ yr), sweeping up a continual supply of fresh disk solids as well as larger solar orbiting planetesimals that are captured into the thin disk by gas drag (cf. McKinnon and Leith 1995).

An alternative model allows Io, Europa, and Ganymede to accrete within the traditional minimum mass, thick subnebula, but appeals to subnebular gas redistribution by satellite–disk torques (gap opening) to alter the overall balance of satellite–disk angular momentum transfer such that these satellites' semi-major axis drifts are substantially slowed or arrested (Mosqueira and Estrada 2003a,b). In the latter model the distant portions of the nebula, beyond the present position of Callisto, are much thinner and accretion proceeds more slowly, forming a large number of small satellites. The small satellites do not remain in position, however, but under the influence of gas drag drift inward to ultimately coalesce into Callisto.

The implications for the initial satellite chemistry of these two models are profound. In the model of Mosqueira and Estrada (2003a,b), the pressure, density, and temperature conditions inward of Callisto's position resemble that of traditional static proto-jovian nebula models (Prinn and Fegley 1989, Lunine and Stevenson 1982). In these models, solar composition gas cools from an initially hot state to at least the water-ice condensation threshold somewhere between the radial positions of Europa and Ganymede. Condensation calculations imply that in thermodynamic equilibrium in such a relatively warm, dense subnebula, mafic silicates, for example, should hydrate to serpentine and iron should oxidize to magnetite, Fe_3O_4 (Prinn and Fegley 1981). In addition, CO and N_2, which in the solar nebula are kinetically inhibited in the gas phase from converting to thermodynamically stable CH_4 and NH_3 (Lewis and Prinn 1980), would be able to convert over the lifetime of the jovian subnebula (Prinn and Fegley 1981, 1989). Moreover, organic matter and graphite, both presolar and of solar nebular ori-

gin, should also vaporize and equilibrate to CH_4. Methane is too volatile to have condensed in this traditional jovian subnebula, and NH_3–H_2O ice can form only in cooler regions farther from Jupiter (possibly affecting Callisto or even Ganymede, but not Europa, which is ice deprived) (Lunine and Stevenson 1982).

In contrast, the gas-starved disk of Canup and Ward (2002) is heated less, and solar nebula solids will be less thermally processed. Even if thermodynamically favored, the hydration and oxidation reactions above are likely to be kinetically inhibited in the gas phase (although they could proceed by means of water–rock reactions within planetesimals or the satellites themselves). Solar CO and N_2 gas will tend to be retained in the subnebula, as will organic matter and graphite. An independent calculation of the kinetics in a model of the saturnian subnebula, based on a numerical simulation of gas inflow at the end of runaway gas accretion by Saturn (Coradini *et al.* 1995) and which yielded a relatively thin subnebula (but not as thin as in Canup and Ward 2002), came to a similar conclusion (i.e., kinetic inhibition) with respect to the thermochemistry of gas-phase C and N (Mousis *et al.* 2002). Similarly, in the thin, cold outer disk of the Mosqueira and Estrada (2003a,b) model, thermochemical equilibration/conversion of solar nebular gases and solids should also be kinetically inhibited.

Essentially, in the gas-starved disk model for all the satellites, and in the thin-outer-disk model for Callisto only, satellite compositions should more resemble those of solar orbiting planetesimals in the Jupiter zone. In terms of asteroid types observed today, the most relevant classes would be the dark, presumably carbonaceous asteroids: C, P, and especially D types, as the latter dominate the Trojan clouds (e.g., Gradie *et al.* 1989). For Europa and Io, dehydrated or partially dehydrated versions of these compositional classes would best apply, because of heating of the infalling planetesimals. For Callisto, both models predict protracted accretion, which is necessary to explain an interior that is only partially differentiated (Anderson *et al.* 2001c,b), for otherwise accretional heat cannot be efficiently radiated away and ice melting followed by rock-from-ice differentiation ensues (see discussions in Schubert *et al.*, 1981; Lunine and Stevenson, 1982; and McKinnon and Parmentier 1986). In this regard, the detailed model proposed by Lunine and Stevenson (1982) to carry accretional heat away from Callisto by means of convection in a thick satellite atmosphere that connects a minimum mass jovian subnebula encounters severe dynamical difficulties due to the strong satellite–disk torques implied (i.e., there would be no tidal gap and satellite migration would be rapid).

The role of accretional heating in the further evolution of the Galilean satellites is somewhat uncertain. Accretional heating alone could have raised the temperature in each of the Galilean satellites by about 1000 K or more (Schubert *et al.* 1986), but uncertainty in how much accretional energy was retained by each satellite has always made it difficult to assess how effective this heat source was in leading to early differentiation of the moons. Apparently, accretional heating was insufficient to fully separate the ice and rock in Callisto which we now know to be partially differentiated, with ice separated from rock only in its outer layers. Moreover, it is not known if the partial separation of ice and rock in Callisto should be attributed to accretional heating at all, since the amount of separation that exists today could be the result of a gradual process driven by radiogenic heating in a convecting ice–rock mixture (Spohn and Breuer 1998, Nagel 2001, Nagel *et al.* 2003). The other Galilean moons are fully differentiated (ice and rock and metal) so it could be that accretional heating played an important role in this. However, there is still uncertainty in when the differentiation of the inner three Galilean satellites occurred, so radiogenic heating over geologic time could have been essential if the differentiation occurred late in the evolution of each moon. Differentiation of Io, Europa and Ganymede could also have been triggered by tidal heating as the satellites evolved through orbital resonance configurations on their way to the present Laplace resonance (Malhotra 1991, Showman and Malhotra 1997, Showman *et al.* 1997). Differentiation itself is not a large energy source for the inner three Galilean satellites, amounting to only about 10% of the maximum accretional energy or about 100–200 K (Schubert *et al.* 1986).

13.9 CONCLUDING COMMENTS

The *Galileo* mission has placed some stringent constraints on models of Galilean satellite evolution that were unknown prior to the mission. The internal structures of the satellites inferred from the gravity data are prominent among the new constraints. The magnetic field of Ganymede, thought to originate in a core dynamo (Schubert *et al.* 1996), requires Ganymede's metallic core not only to be molten (at least in part) but to be convecting at present. The nonexistence of an Ionian magnetic field is just as important to our understanding of dissipative heating in Io and the satellite's internal structure, dynamics and evolution (Wienbruch and Spohn 1995, Spohn 1997). The magnetic field signals of electromagnetic induction from highly electrically conducting layers in the outer parts of Europa, Callisto, and probably Ganymede, require the preservation to the present of internal liquid water oceans in the outer ice shells of these moons. The close-up views of Europa's surface add strong support to the existence of a subsurface liquid water ocean in the satellite. These new constraints on Galilean satellite evolution are yet to be fully exploited.

One way to decide which view of satellite formation, traditional minimum mass nebula or gas-starved disk, is more correct, is to test their predictions for the structure and chemistry of the Galilean satellites. Perhaps the most telling of these tests is whether the divergent structures and evolutions of Ganymede and Callisto can be explained in a natural and economical way.

The exploration of the Galilean moons by the *Galileo* spacecraft has revealed a great deal about the internal structure and interior dynamics of these bodies. These observations have also placed important constraints on the origin and evolution of the satellites. It is not surprising that there are still major questions to be answered. Some of them are:

(1) How did the Galilean satellites form and how did they evolve to their present state?

(2) What is the nature of Io's present thermal and dynamical state?

(3) Is Io's core totally molten at present?

(4) Does Io have a small internal magnetic field?

(5) What is the extent of partial melting in Io's mantle?

(6) How thick is Io's crust and what is its composition? How thick is Io's lithosphere?

(7) How thick is the ice above Europa's subsurface liquid water ocean? How thick is the ocean?

(8) What fraction of Europa's core is solid?

(9) Is Ganymede's core partially frozen?

(10) How does Ganymede generate its magnetic field?

(11) What is the depth dependence of ice/rock fraction in Callisto?

(12) Why is Ganymede fully differentiated (ice from rock from metal) while Callisto's ice and rock+metal have separated only in the outer part of the satellite?

(13) What are the oxidation states of the mantles and cores of Io, Europa, and Ganymede?

(14) Are all the Galilean satellites in hydrostatic equilibrium?

(15) Are there truly liquid water oceans inside Ganymede and Callisto? If yes, how deep and how thick are they?

(16) Does tidal heating in Europa occur in the ice shell or rock mantle or both?

(17) What is the composition of the outer ice shells and oceans on the icy Galilean satellites? Is a significant amount of ammonia dihydrate present?

Acknowledgments. The authors would like to thank Francis Nimmo for a helpful review. We gratefully acknowledge the support of the *Galileo* Project and NASA's Planetary Geology and Geophysics and Jovian System Data Analysis Programs through several grants. We benefited from conversations with William Moore, who prepared Figure 13.3. We thank Eunice L. Lau and Robert A. Jacobson for helpful discussions and for assistance with Tables 13.1 and 13.2. Judy Hohl provided invaluable assistance in the preparation of the manuscript.

REFERENCES

Anderson, J. D., Lectures on physical and technical problems posed by precision radio tracking, in *Experimental Gravitation*, B. Bertotti, ed., pp. 163–199, Academic Press, 1974.

Anderson, J. D., E. L. Lau, W. L. Sjogren, G. Schubert, and W. B. Moore, Gravitational constraints on the internal structure of Ganymede, *Nature* 384, 541–543, 1996a.

Anderson, J. D., W. L. Sjogren, and G. Schubert, *Galileo* gravity results and the internal structure of Io, *Science* **272**, 709–712, 1996b.

Anderson, J. D., E. L. Lau, W. L. Sjogren, G. Schubert, and W. B. Moore, Europa's differentiated internal structure: Inferences from two *Galileo* encounters, *Science* **276**, 1236–1239, 1997.

Anderson, J. D., G. Schubert, R. A. Jacobson, E. L. Lau, W. B. Moore, and W. L. Sjogren, Distribution of rock, metals, and ices in Callisto, *Science* **280**, 1573–1576, 1998a.

Anderson, J. D., G. Schubert, R. A. Jacobson, E. L. Lau, W. B. Moore, and W. L. Sjogren, Europa's differentiated internal structure: Inferences from four *Galileo* encounters, *Science* **281**, 2019–2022, 1998b.

Anderson, J. D., R. A. Jacobson, E. L. Lau, W. B. Moore, O. Olsen, G. Schubert, P. C. Thomas, and *Galileo* Gravity Science Team, Shape, mean radius, gravity field and interior structure of Ganymede, *BAAS* **33**, 1101, 2001a.

Anderson, J. D., R. A. Jacobson, E. L. Lau, W. B. Moore, and G. Schubert, Io's gravity field and interior structure, *J. Geophys. Res.* **106**, 32 963–32 970, 2001b.

Anderson, J. D., R. A. Jacobson, T. P. McElrath, W. B. Moore, G. Schubert, and P. C. Thomas, Shape, mean radius, gravity field and interior structure of Callisto, *Icarus* **153**, 157–161, 2001c.

Anderson, J. D., G. Schubert, A. Anabtawi, R. A. Jacobson, E. L. Lau, and W. B. Moore, Recent results on Io's gravity field and interior structure, *Eos* p. S212, 2002.

Archinal, B. A., M. E. Davies, T. R. Colvin, T. L. Becker, R. L. Kirk, and A. R. Gitlin, An improved RAND–USGS control network and size determination for Io, in *Lunar and Planetary Science Conference Abstracts*, p. 1746, 2001.

Boehler, R., The phase diagram of iron to 430 kbar, *Geophys. Res. Lett.* **13**, 1153–1156, 1986.

Boehler, R., Melting of the Fe–FeO and Fe–FeS systems at high pressure: Constraints on core temperatures, *Earth Planet. Sci. Lett.* **111**, 217–227, 1992.

Boehler, R., Melting temperature of the Earth's mantle and core: Earth's thermal structure, *Ann. Rev. Earth Planet. Sci.* **24**, 15–40, 1996.

Boehler, R., High-pressure experiments and the phase diagram of lower mantle and core materials, *Rev. Geophys.* **38**, 221–245, 2000.

Bryden, G., X. Chen, D. N. C. Lin, R. P. Nelson, and J. C. B. Papaloizou, Tidally induced gap formation in protostellar disks: Gap clearing and suppression of protoplanetary growth, *ApJ* **514**, 344–367, 1999.

Buffett, B. A., H. E. Huppert, J. R. Lister, and A. W. Woods, On the thermal evolution of the Earth's core, *J. Geophys. Res.* **101**, 7989–8006, 1996.

Campbell, J. K. and S. P. Synnott, Gravity field of the jovian system from *Pioneer* and *Voyager* tracking data, *AJ* **90**, 364–372, 1985.

Canup, R. M. and W. R. Ward, Formation of the Galilean satellites: Conditions of accretion, *AJ* **124**, 3404–3423, 2002.

Carr, M. H., M. J. S. Belton, C. R. Chapman, M. E. Davies, P. Geissler, R. Greenberg, A. S. McEwen, B. R. Tufts, R. Greeley, and R. Sullivan, Evidence for a subsurface ocean on Europa, *Nature* **391**, 363–365, 1998a.

Carr, M. H., A. S. McEwen, K. A. Howard, F. C. Chuang, P. Thomas, P. Schuster, J. Oberst, G. Neukum, G. Schubert, and the *Galileo* Imaging Team, Mountains and calderas on Io: Possible implications for lithosphere structure and magma generation, *Icarus* **135**, 146–165, 1998b.

Cassen, P., R. T. Reynolds, and S. J. Peale, Is there liquid water on Europa?, *Geophys. Res. Lett.* **6**, 731–734, 1979.

Cassen, P., S. J. Peale, and R. T. Reynolds, Tidal dissipation in Europa: A correction, *Geophys. Res. Lett.* **7**, 987–988, 1980.

Chizov, V. E., Thermodynamic properties and equation of state of high-pressure ice phases, *Prikladnay Mekhanika i Tekhnicheskaya Fizika* **2**, 113–123, 1993.

Cohen, E. R. and B. N. Taylor, The fundamental physical constants, *Phys. Today* **52**, BG5–BG9, 1999.

Consolmagno, G. J., Io: Thermal models and chemical evolution, *Icarus* **47**, 36–45, 1981.

Consolmagno, G. J. and J. S. Lewis, Preliminary thermal history models of icy satellites, in *Planetary Satellites*, J. A. Burns (ed), University of Arizona Press, pp. 492–500, 1977.

Coradini, A., P. Cerroni, G. Magni, and C. Federico, Formation of the satellites of the outer solar system: Sources of their atmospheres, in *Origin and Evolution of Planetary and Satellite Atmospheres*, pp. 723–762, 1989.

Coradini, A., C. Federico, O. Forni, and G. Magni, Origin and thermal evolution of icy satellites, *Surv. Geophys.* **16**, 533–591, 1995.

Crary, F. J. and F. Bagenal, Remanent ferromagnetism and the interior structure of Ganymede, *J. Geophys. Res.* **103**, 25 757–25 774, 1998.

Danby, J. M. A., *Fundamentals of Celestial Mechanics*, Willmann-Bell, 1988.

Davies, M. E., T. R. Colvin, J. Oberst, W. Zeitler, P. Schuster, G. Neukum, A. S. McEwen, C. B. Phillips, P. C. Thomas, J. Veverka, M. J. S. Belton, and G. Schubert, The control networks of the Galilean satellites and implications for global shape, *Icarus* **135**, 372–376, 1998.

Deschamps, F. and C. Sotin, Thermal convection in the outer shell of large icy satellites, *J. Geophys. Res.* **106**, 5107–5121, 2001.

Durham, W. B. and L. A. Stern, Rheological properties of water ice: applications to satellites of the outer planets, *Ann. Rev. Earth Planet. Sci.* **29**, 295–330, 2001.

Durham, W. B., S. H. Kirby, and L. A. Stern, Creep of water ices at planetary conditions: A compilation, *J. Geophys. Res.* **102**, 16 293–16 302, 1997.

Durham, W. B., S. H. Kirby, and L. A. Stern, Rheology of planetary ices, in *Solar System ices*, p. 63, 1998.

Durham, W. B., L. A. Stern, and S. H. Kirby, Rheology of ice I at low stress and elevated confining pressure, *J. Geophys. Res.* **106**, 11 031–11 042, 2001.

Fanale, F. P., T. V. Johnson, and D. L. Matson, Io's surface and the histories of the Galilean satellites, in *Planetary Satellites*, J. A. Burns (ed), University of Arizona Press, pp. 379–405, 1977.

Fanale, F. P., J. R. Salvail, D. L. Matson, and R. H. Brown, The effect of volume phase changes, mass transport, sunlight penetration, and densification on the thermal regime of icy regoliths, *Icarus* **88**, 193–204, 1990.

Fei, Y., C. M. Bertka, and L. W. Finger, High-pressure iron–sulfur compound, Fe_3S_2 and melting relations in the Fe–FeS system, *Science* **275**, 1621–1623, 1997.

Fischer, H.-J. and T. Spohn, Thermal-orbital histories of viscoelastic models of Io (J1), *Icarus* **83**, 39–65, 1990.

Folkner, W. M., C. F. Yoder, D. N. Yuan, E. M. Standish, and R. A. Preston, Interior structure and seasonal mass redistribution of Mars from radio tracking of Mars *Pathfinder*, *Science* **278**, 1749–1752, 1997.

Friedson, A. J. and D. J. Stevenson, Viscosity of rock–ice mixtures and applications to the evolution of icy satellites, *Icarus* **56**, 1–14, 1983.

Gaskell, R. W., S. P. Synnott, A. S. McEwen, and G. G. Schaber, Large-scale topography of Io: Implications for internal structure and heat transfer, *Geophys. Res. Lett.* **15**, 581–584, 1988.

Geissler, P. E., R. Greenberg, G. Hoppa, P. Helfenstein, A. McEwen, R. Pappalardo, R. Tufts, M. Ockert-Bell, R. Sullivan, and R. Greeley, Evidence for non-synchronous rotation of Europa, *Nature* **391**, 368–370, 1998.

Gessmann, C. K. and B. J. Wood, Potassium in the Earth's core?, *Earth Planet. Sci. Lett.* **200**, 63–78, 2002.

Goldsby, D. L. and D. L. Kohlstedt, Grain boundary sliding in fine-grained ice I, *Scripta Materialia* **37**, 1399–1406, 1997.

Goldsby, D. L. and D. L. Kohlstedt, Superplastic deformation of ice: Experimental observations, *J. Geophys. Res.* **106**, 11 017–11 030, 2001.

Gradie, J. C., C. R. Chapman, and E. F. Tedesco, Distribution of taxonomic classes and the compositional structure of the asteroid belt, in *Asteroids II*, pp. 316–335, 1989.

Grasset, O. and E. M. Parmentier, Thermal convection in a volumetrically heated, infinite Prandtl number fluid with strongly temperature-dependent viscosity: Implications for planetary evolution, *J. Geophys. Res.* **103**, 18 171–18 181, 1998.

Grasset, O. and C. Sotin, The cooling rate of a liquid shell in Titan's interior, *Icarus* **123**, 101–112, 1996.

Greenberg, R., Orbital evolution of the Galilean satellites, in *Satellites of Jupiter*, D. A. Morrison, University of Arizona Press, pp. 65–92, 1982.

Greenberg, R., P. Geissler, G. Hoppa, B. R. Tufts, D. D. Durda, R. Pappalardo, J. W. Head, R. Greeley, R. Sullivan, and M. H. Carr, Tectonic processes on Europa: Tidal stresses, mechanical response, and visible features, *Icarus* **135**, 64–78, 1998.

Greenberg, R., P. Geissler, B. R. Tufts, and G. V. Hoppa, Habitability of Europa's crust: The role of tidal-tectonic processes, *J. Geophys. Res.* **105**, 17 551–17 562, 2000.

Gubbins, D., T. G. Masters, and J. A. Jacobs, Thermal evolution of the Earth's core, *Geophys. J. R. Astron. Soc.* **59**, 5–99, 1979.

Gurnett, D. A., W. S. Kurth, A. Roux, S. J. Bolton, and C. F. Kennel, Evidence for a magnetosphere at Ganymede from the plasma-wave observations by the *Galileo* spacecraft, *Nature* **384**, 535–537, 1996.

Hogenboom, D. L., J. S. Kargel, J. P. Ganasan, and L. Lee, Magnesium sulfate-water to 400 MPa using a novel piezometer: Densities, phase equilibria, and planetological implications, *Icarus* **115**, 258–277, 1995.

Hogenboom, D. L., J. S. Kargel, G. J. Consolmagno, T. C. Holden, L. Lee, and M. Buyyounouski, The ammonia–water system and the chemical differentiation of icy satellites, *Icarus* **128**, 171–180, 1997.

Hoppa, G., R. Greenberg, B. R. Tufts, P. Geissler, C. Phillips, and M. Milazzo, Distribution of strike-slip faults on Europa, *J. Geophys. Res.* **105**, 22 617–22 628, 2000.

Hoppa, G. V., B. R. Tufts, R. Greenberg, and P. E. Geissler, Formation of cycloidal features on Europa, *Science* **285**, 1899–1902, 1999.

Hubbard, W. B. and J. D. Anderson, Possible flyby measurements of Galilean satellite interior structure, *Icarus* **33**, 336–341, 1978.

Hussmann, H., T. Spohn, and K. Wieczerkowski, Thermal equilibrium states of Europa's ice shell: Implications for internal ocean thickness and surface heat flow, *Icarus* **156**, 143–151, 2002.

Iess, L., G. Giampieri, J. D. Anderson, and B. Bertotti, Doppler measurement of the solar gravitational deflection, *Class. Quantum Grav.* **16**, 1487–1502, 1999.

Jacobson, R. A., *Pioneer* and *Voyager* Jupiter Encounter Orbit Reconstruction in the ICRF System, in *AAS/AIAA Space Flight Mechanics Meeting*, 2002. Paper 02–157.

Kargel, J. S., Ammonia–water volcanism on icy satellites: Phase relations at 1 atmosphere, *Icarus* **100**, 556–574, 1992.

Kargel, J. S., Physical chemistry of ices in the outer solar system, in *Solar System Ices*, B. Schmitt, C. de Bergh, and M. Festou, eds., pp. 3–32, Kluwer, 1998.

Kargel, J. S., S. K. Croft, J. L. Lunine, and J. S. Lewis, Rheological properties of ammonia–water liquids and crystal–liquid slurries: Planetological applications, *Icarus* **89**, 93–112, 1991.

Kargel, J. S., J. Z. Kaye, J. W. Head, G. M. Marion, R. Sassen, J. K. Crowley, O. P. Ballesteros, S. A. Grant, and D. L. Hogenboom, Europa's crust and ocean: Origin, composition, and the prospects for life, *Icarus* **148**, 226–265, 2000.

Kattenhorn, S. A., Nonsynchronous rotation evidence and fracture history in the Bright Plains Region, Europa, *Icarus* **157**, 490–506, 2002.

Kaula, W. M., *Theory of Satellite Geodesy: Applications of Satellites to Geodesy*, Waltham, 1966.

Kaula, W. M., *An Introduction to Planetary Physics: The Terrestrial Planets*, Wiley, 1968.

Keszthelyi, L., W. L. Jaeger, A. S. McEwen, and E. P. Turtle, Io's interior: A synthesis view at the end of the *Galileo* era, in *Lunar and Planetary Science Conference Abstracts*, p. 1760, 2003.

Khurana, K. K., M. G. Kivelson, and C. T. Russell, Interaction of Io with its torus: Does Io have an internal magnetic field?, *Geophys. Res. Lett.* **24**, 2391–2394, 1997a.

Khurana, K. K., M. G. Kivelson, C. T. Russell, R. J. Walker, and D. J. Southwood, Absence of an internal magnetic field at Callisto, *Nature* **387**, 262–264, 1997b.

Khurana, K. K., M. G. Kivelson, D. J. Stevenson, G. Schubert, C. T. Russell, R. J. Walker, S. Joy, and C. Polanskey, Induced magnetic fields as evidence for subsurface oceans in Europa and Callisto, *Nature* **395**, 777–780, 1998.

Kirk, R. L. and D. J. Stevenson, Thermal evolution of a differentiated Ganymede and implications for surface features, *Icarus* **69**, 91–134, 1987.

Kivelson, M. G., K. K. Khurana, C. T. Russell, R. J. Walker, J. Warnecke, F. V. Coroniti, C. Polanskey, D. J. Southwood, and G. Schubert, Discovery of Ganymede's magnetic field by the *Galileo* spacecraft, *Nature* **384**, 537–541, 1996a.

Kivelson, M. G., K. K. Khurana, R. J. Walker, J. A. Linker, C. R. Russell, D. J. Southwood, and C. Polanskey, A magnetic signature at Io: Initial report from the *Galileo* magnetometer, *Science* **273**, 337–340, 1996b.

Kivelson, M. G., J. Warnecke, L. Bennet, L. Joy, K. K. Khurana, J. A. Linker, C. T. Russell, R. J. Walker, and C. Polanskey, Ganymede's magnetosphere: Magnetometer overview, *J. Geophys. Res.* **103**, 19 963–19 972, 1998.

Kivelson, M. G., K. K. Khurana, D. J. Stevenson, L. Bennett, S. Joy, C. T. Russell, R. J. Walker, C. Zimmer, and C. Polanskey, Europa and Callisto: Induced or intrinsic fields in a periodically varying plasma environment, *J. Geophys. Res.* **104**, 4609–4625, 1999.

Kivelson, M. G., K. K. Khurana, C. T. Russell, M. Volwerk, R. J. Walker, and C. Zimmer, *Galileo* magnetometer measurements: A stronger case for a subsurface ocean at Europa, *Science* **289**, 1340–1343, 2000.

Kivelson, M. G., K. K. Khurana, R. Lopes, and E. Turtle, Polar passes by Io: Limits on the internal field and sources of field-aligned currents in the polar cap, *Eos* pp. A3+, 2002a.

Kivelson, M. G., K. K. Khurana, and M. Volwerk, The permanent and inductive magnetic moments of Ganymede, *Icarus* **157**, 507–522, 2002b.

Kliore, A. J., D. P. Hinson, F. F. M., A. F. Nagy, and T. E. Cravens, The ionosphere of Europa from *Galileo* radio occultations, *Science* **277**, 355–358, 1997.

Konrad, W. and T. Spohn, Thermal history of the Moon: Implications for an early core dynamo and post-accretional magmatism, *Adv. Space Res.* **10**, 1511–1521, 1997.

Korycansky, D. G., J. B. Pollack, and P. Bodenheimer, Numerical models of giant planet formation with rotation, *Icarus* **92**, 234–251, 1991.

Kuang, Z. and D. J. Stevenson, Core sizes and internal structure of Earth's and Jupiter's satellites, *Eos* **77**, F437, 1996. Fall Meeting Supplement.

Kuskov, O. L. and V. A. Kronrod, Core sizes and internal structure of Earth's and Jupiter's satellites, *Icarus* **151**, 204–227, 2001a.

Kuskov, O. L. and V. A. Kronrod, L- and LL-chondritic models of the chemical composition of Io, *Solar System Res.* **35**, 198–208, 2001b.

Lawson, C. L. and R. J. Hanson, *Solving Least Squares Problems*, Prentice-Hall, 1974.

Lewis, J. S., Io: Geochemistry of sulfur, *Icarus* **50**, 103–114, 1982.

Lewis, J. S. and P. G. Prinn, Kinetic inhibition of CO and N_2 reduction in the solar nebula, *ApJ* **238**, 357–364, 1980.

Lodders, K. and B. Fegley, *The Planetary Scientist's Companion*, Oxford University Press, 1998.

Lopes-Gautier, R., A. S. McEwen, W. B. Smythe, P. E. Geissler, L. Kamp, A. G. Davies, J. R. Spencer, L. Keszthelyi, R. Carlson, F. E. Leader, R. Mehlman, L. Soderblom, T. *Galileo*. NIMS, and S. Teams, Active volcanism on Io: Global distribution and variations in activity, *Icarus* **140**, 243–264, 1999.

Lubow, S. H., M. Seibert, and P. Artymowicz, Disk accretion onto high-mass planets, *ApJ* **526**, 1001–1012, 1999.

Lunine, J. I. and D. J. Stevenson, Formation of the Galilean satellites in a gaseous nebula, *Icarus* **52**, 14–39, 1982.

Malhotra, R., Tidal origin of the Laplace resonance and the resurfacing of Ganymede, *Icarus* **94**, 399–412, 1991.

Matson, D. L., T. V. Johnson, G. J. Veeder, D. L. Blaney, and A. G. Davies, Upper bound on Io's heat flow, *J. Geophys. Res.* **106**, 33 021–33 024, 2001.

McCord, T. B., G. B. Hansen, F. P. Fanale, R. W. Carlson, D. L. Matson, T. V. Johnson, W. D. Smythe, J. K. Crowley, P. D. Martin, A. Ocampo, C. A. Hibbits, J. C. Granahan, and the NIMS Team, Salts on Europa's surface detected by *Galileo*'s near infrared mapping spectrometer, *Science* **280**, 1242–1245, 1998.

McEwen, A. S., J. I. Lunine, and M. H. Carr, Dynamic Geophysics of Io, in *Time Variable Phenomena in the Jovian System*, NASA-SP-494, pp. 11–46, 1989.

McEwen, A. S., L. Keszthelyi, P. Geissler, D. P. Simonelli, M. H. Carr, T. V. Johnson, K. P. Klaasen, H. H. Breneman, T. J. Jones, J. M. Kaufman, K. P. Magee, D. A. Senske, M. J. S. Belton, and G. Schubert, Active volcanism on Io as seen by *Galileo* SSI, *Icarus* **135**, 181–219, 1998a.

McEwen, A. S., L. Keszthelyi, J. R. Spencer, G. Schubert, D. L. Matson, R. Lopes-Gautier, K. P. Klaasen, T. V. Johnson, J. W. Head, P. Geissler, S. Fagents, A. G. Davies, M. H. Carr, H. H. Breneman, and M. J. S. Belton, High-temperature silicate volcanism on Jupiter's moon Io, *Science* **281**, 87–90, 1998b.

McEwen, A. S., M. J. S. Belton, H. H. Breneman, S. A. Fagents, P. Geissler, R. Greeley, J. W. Head, G. Hoppa, W. L. Jaeger, T. V. Johnson, L. Keszthelyi, K. P. Klaasen, R. Lopes-Gautier, K. P. Magee, M. P. Milazzo, J. M. Moore, R. T. Pappalardo, C. B. Phillips, J. Radebaugh, G. Schubert, P. Schuster, D. P. Simonelli, R. Sullivan, P. C. Thomas, E. P. Turtle, and D. A. Williams, *Galileo* at Io: Results from High-Resolution Imaging, *Science* **288**, 1193–1198, 2000.

McKinnon, W., Geodynamics of Icy Satellites, in *Solar System Ices*, pp. 525–549, 1998.

McKinnon, W. B., Core evolution in the icy Galilean satellites, and the prospects for dynamo-generated magnetic fields, *BAAS* **28**, 1076, 1996.

McKinnon, W. B., Mystery of Callisto: Is it undifferentiated?, *Icarus* **130**, 540–543, 1997.

McKinnon, W. B. and S. Desai, Internal structures of the Galilean satellites: What can we really tell?, in *Lunar and Planetary Institute Conference Abstracts*, p. 2104, 2003.

McKinnon, W. B. and A. C. Leith, Gas drag and the orbital evolution of a captured Triton, *Icarus* **118**, 392–413, 1995.

McKinnon, W. B. and E. M. Parmentier, Ganymede and Callisto, in *Satellites*, J. A. Burns, M. S. Matthews (eds), University of Arizona Press, pp. 718–763, 1986.

Monnereau, M. and F. Dubuffet, Is Io's mantle really molten?, *Icarus* **158**, 450–459, 2002.

Moore, J. M., E. Asphaug, M. J. S. Belton, B. Bierhaus, H. H. Breneman, S. M. Brooks, C. R. Chapman, F. C. Chuang, G. C. Collins, B. Giese, R. Greeley, J. W. Head, S. Kadel, K. P. Klaasen, J. E. Klemaszewski, K. P. Magee, J. Moreau, D. Morrison, G. Neukum, R. T. Pappalardo, C. B. Phillips, P. M. Schenk, D. A. Senske, R. J. Sullivan, E. P. Turtle, and K. K. Williams, Impact Features on Europa: Results of the *Galileo* Europa Mission (GEM), *Icarus* **151**, 93–111, 2001.

Moore, W. B., The thermal state of Io, *Icarus* **154**, 548–550, 2001.

Moore, W. B., Tidal heating and convection in Io, *J. Geophys. Res.* **in press** 2003.

Moore, W. B. and G. Schubert, The tidal response of Europa, *Icarus* **147**, 317–319, 2000.

Mosqueira, I. and P. R. Estrada, Formation of the regular satellites of giant planets in an extended gaseous nebula: I. Subnebula model and accretion of satellites, *Icarus* **163**, 198–231, 2003a.

Mosqueira, I. and P. R. Estrada, Formation of the regular satellites of giant planets in an extended gaseous nebula: II. Satellite migration and survival, *Icarus* **163**, 232–255, 2003b.

Mousis, O., D. Gautier, and D. Bockelée-Morvan, An evolutionary turbulent model of Saturn's subnebula: Implications for the origin of the atmosphere of Titan, *Icarus* **156**, 162–175, 2002.

Moyer, T. D., Formulation for observed and computed values of Deep Space Network data types for navigation, in *DESCANSO 2*, JPL, 2000.

Mueller, S. and W. B. McKinnon, Three-layered models of Ganymede and Callisto: Compositions, structures, and aspects of evolution, *Icarus* **76**, 437–464, 1988.

Nagel, K., *Thermal-Compositional Convection and the Differentiation Process in Callisto*, Ph.D. thesis, University of Münster, 2001.

Nagel, K., D. Breuer, and T. Spohn, A model for the interior structure, evolution and differentiation of Callisto, *Icarus* **submitted**, 2003.

Naldrett, A. J., A portion of the system Fe–S–O between 900 and 1080°C and its application to sulfide ore magmas, *J. Petrol.* **10**, 171–201, 1969.

Neubauer, F., Oceans inside Jupiter's moons, *Nature* **395**, 749–751, 1998.

Nimmo, F. and M. Manga, Causes, characteristics and consequences of convective diapirism on Europa, *Geophys. Res. Lett.* **29**, 2109, doi:10.1029/2002GL015,754, 2002.

Nimmo, F., B. Giese, and R. T. Pappalardo, Estimates of Europa's ice shell thickness from elastically-supported topography, *Geophys. Res. Lett.* **30**, 1233, doi:10.1029/2002GL016,660, 2003.

Ojakangas, G. W. and D. J. Stevenson, Thermal state of an ice shell on Europa, *Icarus* **81**, 220–241, 1989.

O'Leary, B. and T. C. van Flandern, Io's triaxial figure, *Icarus* **17**, 209–215, 1972.

O'Reilly, T. C. and G. F. Davies, Magma transport of heat on Io: A mechanism allowing a thick lithosphere, *Geophys. Res. Lett.* **8**, 313–316, 1981.

Pappalardo, R. T., J. W. Head, R. Greeley, R. J. Sullivan, C. Pilcher, G. Schubert, W. B. Moore, M. H. Carr, J. M. Moore, and M. J. S. Belton, Geological evidence for solid-state convection in Europa's ice shell, *Nature* **391**, 365–368, 1998.

Pappalardo, R. T., M. J. S. Belton, H. H. Breneman, M. H. Carr, C. R. Chapman, G. C. Collins, T. Denk, S. Fagents, P. E. Geissler, B. Giese, R. Greeley, R. Greenberg, J. W. Head, P. Helfenstein, G. Hoppa, S. D. Kadel, K. P. Klaasen, J. E. Klemaszewski, K. Magee, A. S. McEwen, J. M. Moore, W. B. Moore, G. Neukum, C. B. Phillips, L. M. Prockter, G. Schubert, D. A. Senske, R. J. Sullivan, B. R. Tufts, E. P. Turtle, R. Wagner, and K. K. Williams, Does Europa have a subsurface ocean? Evaluation of the geological evidence, *J. Geophys. Res.* **104**, 24 015–24 055, 1999.

Peale, S. J., Origin and evolution of the natural satellites, *ARA&A* **37**, 533–602, 1999.

Peale, S. J. and M. H. Lee, A primordial origin of the Laplace relation among the Galilean satellites, *Science* **298**, 593–597, 2002.

Peale, S. J., P. Cassen, and R. T. Reynolds, Melting of Io by tidal dissipation, *Science* **203**, 892–894, 1979.

Pollack, J. B. and F. Fanale, Origin and evolution of the Jupiter satellite system, in *Satellites of Jupiter*, D. Morrison (ed), University of Arizona Press, pp. 872–891, 1982.

Pollack, J. B., J. I. Lunine, and W. C. Tittemore, Origin of the uranian satellites, in *Uranus*, J. T. Bergstralh, E. D. Miner, M. S. Matthews (eds), University of Arizona Press, pp. 469–512, 1991.

Pollack, J. B., O. Hubickyj, P. Bodenheimer, J. J. Lissauer, M. Podolak, and Y. Greenzweig, Formation of the giant planets by concurrent accretion of solids and gases, *Icarus* **124**, 62–85, 1996.

Prinn, R. G. and B. Fegley, Kinetic inhibition of CO and N_2 reduction in circumplanetary nebulae: Implications for satellite composition, *ApJ* **249**, 308–317, 1981.

Prinn, R. G. and B. Fegley, Origin of planetary, satellite, and cometary volatiles, in *Origin and Evolution of Planetary and Satellite Atmospheres*, S. K. Atreya, J. B. Pollack, and M. S. Matthews, eds, pp. 8–136, University of Arizona Press, 1989.

Rama Murthy, V., W. van Westrenen, and Y. Fei, Experimental evidence that potassium is a substantial radioactive heat source in planetary cores, Nature **423**, 163–165, 2003.

Rappaport, N., B. Bertotti, G. Giampieri, and J. D. Anderson, Doppler measurements of the quadrupole moments of Titan, *Icarus* **126**, 313–323, 1997.

Reynolds, R. T. and P. M. Cassen, On the internal structure of the major satellites of the outer planets, *Geophys. Res. Lett.* **6**, 121–124, 1979.

Ross, M. N. and G. Schubert, Tidal heating in an internal ocean model of Europa, *Nature* **325**, 133–134, 1987.

Ross, M. N., G. Schubert, T. Spohn, and R. W. Gaskell, Internal structure of Io and the global distribution of its topography, *Icarus* **85**, 309–325, 1990.

Ruiz, J., The stability against freezing of an internal liquid-water ocean in Callisto, *Nature* **412**, 409–411, 2001.

Sarson, G. R., C. A. Jones, K. Zhang, and G. Schubert, Magnetoconvection dynamos and the magnetic fields of Io and Ganymede, *Science* **276**, 1106–1108, 1997.

Schenk, P., H. Hargitai, R. Wilson, A. McEwen, and P. Thomas, The mountains of Io: Global and geological perspectives from *Voyager* and *Galileo*, *J. Geophys. Res.* **106**, 33 201–33 222, 2001a.

Schenk, P. M., Thickness constraints on the icy shells of the Galilean satellites from a comparison of crater shapes, *Nature* **417**, 419–421, 2002.

Schenk, P. M., W. B. McKinnon, D. Gwynn, and J. M. Moore, Ganymede's bright terrains by low-viscosity water-ice levels, *Nature* **410**, 57–60, 2001b.

Schilling, N., K. K. Khurana, and M. G. Kivelson, Limits on the intrinsic dipole moment in Europa, *J. Geophys. Res.* **submitted**, 2003.

Schubert, G. and R. L. Walterscheid, Earth, in *Allen's Astrophysical Quantities*, A. N. Cox, ed., pp. 239–292, Springer-Verlag, 2000.

Schubert, G., D. Stevenson, and K. Ellsworth, Internal structures of the Galilean satellites, *Icarus* **47**, 46–59, 1981.

Schubert, G., T. Spohn, and R. T. Reynolds, Thermal histories, compositions and internal structures of the moons of the solar system, in *Satellites*, J. A. Burns and M. S. Matthews, eds, pp. 224–292, University of Arizona Press, 1986.

Schubert, G., K. Zhang, M. G. Kivelson, and J. D. Anderson, The magnetic field and internal structure of Ganymede, *Nature* **384**, 544–545, 1996.

Schubert, G., D. L. Turcotte, and P. Olson, *Mantle Convection in the Earth and Planets*, Cambridge University Press, 2001.

Scott, H. P., Q. Williams, and F. J. Ryerson, Experimental constraints on the chemical evolution of large icy satellites, *Earth Planet. Sci. Lett.* **203**, 399–412, 2002.

Segatz, M., T. Spohn, M. N. Ross, and G. Schubert, Tidal dissipation, surface heat flow, and figure of viscoelastic models of Io, *Icarus* **75**, 187–206, 1988.

Seidelmann, P. K., V. K. Abalakin, M. Bursa, M. E. Davies, C. d. Bergh, J. H. Lieske, J. Oberst, J. L. Simon, E. M. Standish, P. Stooke, and P. C. Thomas, Report of the IAU/IAG Working Group on cartographic coordinates and rotational elements of the planets and satellites: 2000, *Celestial Mechanics and Dynamical Astronomy* **82**, 83–111, 2002.

Showman, A. P. and R. Malhotra, Tidal evolution into the

Laplace resonance and the resurfacing of Ganymede, *Icarus* **127**, 93–111, 1997.

Showman, A. P., D. J. Stevenson, and R. Malhotra, Coupled orbital and thermal evolution of Ganymede, *Icarus* **129**, 367–383, 1997.

Sohl, F., T. Spohn, D. Breuer, and K. Nagel, Implications from *Galileo* observations on the interior structure and chemistry of the Galilean satellites, *Icarus* **157**, 104–119, 2002.

Solomatov, V. S., Scaling of temperature- and stress-dependent viscosity convection, *Phys. Fluids* **7**, 266–274, 1995.

Solomatov, V. S. and L.-N. Moresi, Scaling of time-dependent stagnant lid convection: Application to small-scale convection on Earth and other terrestrial planets, *J. Geophys. Res.* **105**, 21 795–21 818, 2000.

Sotin, C., O. Grasset, and S. Beauchesne, Thermodynamical properties of high pressure ices: Implications for the dynamics and internal structure of large icy satellites, in *Solar System Ices*, pp. 79–96, 1998.

Spaun, N. A., J. W. Head, G. C. Collins, L. M. Prockter, and R. T. Pappalardo, Conamara Chaos region, Europa: Reconstruction of mobile polygonal ice blocks, *Geophys. Res. Lett.* **25**, 4277–4280, 1998.

Spencer, J. R., J. A. Rathbun, L. D. Travis, K. Tamppari, L. Barnard, T. Z. Martin, and A. S. McEwen, Io's thermal emission from the *Galileo* photopolarimeter-radiometer, *Science* **288**, 1198–1201, 2000.

Spohn, T., Tides of Io, in *Tidal Phenomena*, pp. 345–377, 1997.

Spohn, T. and D. Breuer, Implications from Galileo observations on the interior structure and evolution of the Galilean satellites, in *Planetary Systems: The long view*, J. T. T. V. L. Celnikier, ed., pp. 135–144, Editions Frontieres, 1998.

Spohn, T. and G. Schubert, Oceans in the icy Galilean satellites of Jupiter?, *Icarus* **161**, 456–467, 2003.

Spohn, T., W. Konrad, D. Breuer, and R. Ziethe, The longevity of lunar volcanism: Implications of thermal evolution calculations with 2D and 3D mantle convection models, *Icarus* **149**, 54–65, 2001.

Squyres, S. W., R. T. Reynolds, and P. M. Cassen, Liquid water and active resurfacing on Europa, *Nature* **301**, 225–226, 1983.

Stacey, F. D., *Physics of the Earth*, Brookfield, 1992.

Stern, L. A., W. B. Durham, and S. H. Kirby, Grain-size-induced weakening of H_2O ices I and II and associated anisotropic recrystallization, *J. Geophys. Res.* **102**, 5313–5325, 1997.

Stevenson, D. J., Heterogeneous tidal deformation and geysers on Europa, in *Europa Ocean Conference*, San Juan Capistrano, 1996a.

Stevenson, D. J., When *Galileo* met Ganymede, *Nature* **384**, 511–512, 1996b.

Stevenson, D. J., Jupiter and its moons, *Science* **294**, 71–72, 2001.

Stevenson, D. J., Tidal response and stability of two-phase media: Implications for Io, Europa and Titan, *Eos* p. C10, 2002.

Stevenson, D. J. and S. C. McNamara, Background heatflow on hotspot planets: Io and Venus, *Geophys. Res. Lett.* **15**, 1455–1458, 1988.

Stevenson, D. J., T. Spohn, and G. Schubert, Magnetism and thermal evolution of the terrestrial planets, *Icarus* **54**, 466–489, 1983.

Stevenson, D. J., A. W. Harris, and J. I. Lunine, Origins of satellites, in *Satellites*, J. A. Burns, M. S. Matthews (eds), University of Arizona Press, pp. 39–88, 1986.

Sullivan, R., R. Greeley, K. Homan, J. Klemaszewski, M. J. S. Belton, M. H. Carr, C. R. Chapman, R. Tufts, J. W. Head, and R. Pappalardo, Episodic plate separation and fracture infill on the surface of Europa, *Nature* **391**, 371–373, 1998.

Tackley, P. J., G. Schubert, G. A. Glatzmaier, P. Schenk, J. T. Ratcliff, and J.-P. Matas, Three-dimensional simulations of mantle convection in Io, *Icarus* **149**, 79–93, 2001.

Takahashi, E., Melting of a dry peridotite KLB-1 up to 14 GPa: Implications on the origin of peridotitic upper mantle, *J. Geophys. Res.* **91**, 9367–9382, 1986.

Takahashi, E., Speculations on the Archean mantle, *J. Geophys. Res.* **95**, 15 941–15 954, 1990.

Tapley, B. D., Statistical orbit determination theory, in *Recent Advances in Dynamical Astronomy*, B. D. Tapley and V. Szebehely, eds, pp. 396–425, Reidel, 1973.

Tholen, D. J., V. G. Tejfel, and A. N. Cox, Planets and satellites, in *Allen's Astrophysical Quantities*, A. N. Cox, ed., pp. 293–314, Springer-Verlag, 4th edn, 2000.

Thomas, P. C., M. E. Davies, T. R. Colvin, J. Oberst, P. Schuster, G. Neukum, M. H. Carr, A. McEwen, G. Schubert, M. J. S. Belton, and the *Galileo* Imaging Team, The shape of Io from *Galileo* limb measurements, *Icarus* **135**, 175–180, 1998.

Tufts, B. R., R. Greenberg, G. Hoppa, and P. Geissler, Lithospheric dilation on Europa, *Icarus* **146**, 75–97, 2000.

Turcotte, D. L., Magma migration, *Ann. Rev. Earth Planet. Sci.* **10**, 397–408, 1982.

Turcotte, D. L. and G. Schubert, *Geodynamics*, Cambridge University Press, 2002.

Usselman, T. M., Experimental approach to the state of the core. Part 2. Composition and thermal regime, *Am. J. Sci.* **275**, 291–303, 1975a.

Usselman, T. M., Experimental approach to the state of the core. Part I. The liquidus relations of the Fe-rich portion of the Fe–Ni–S system from 30 to 100 kb, *Am. J. Sci.* **275**, 278–290, 1975b.

Veeder, G. J., D. L. Matson, T. V. Johnson, D. L. Blaney, and J. D. Goguen, Io's heat flow from infrared radiometry: 1983–1993, *J. Geophys. Res.* **99**, 17 095–17 162, 1994.

Ward, W. R. and J. M. Hahn, Disk–planet interactions and the formation of planetary systems, *Protostars and Planets IV* pp. 1135–1159, 2000.

Webb, E. K. and D. J. Stevenson, Subsidence of topography on Io, *Icarus* **70**, 348–353, 1987.

Wienbruch, U. and T. Spohn, A self sustained magnetic field on Io?, *Planet. Space Sci.* **43**, 1045–1057, 1995.

Williams, D. A., J. E. Klemaszewski, F. C. Chuang, and R. Greeley, *Galileo* imaging observations of the Valhalla Antipode: Support for a subsurface ocean on Callisto?, *BAAS* **33**, 1100, 2001.

Wu, X., Y. E. Bar-Sever, W. M. Folkner, J. G. Williams, and J. F. Zumberge, Probing Europa's hidden ocean from tidal effects on orbital dynamics, *Geophys. Res. Lett.* **28**, 2245–2248, 2001.

Wyllie, P. J., Magma genesis, plate tectonics, and chemical differentiation of the Earth, *Rev. Geophys.* **26**, 370–404, 1988.

Yoder, C. F., How tidal heating in Io drives the Galilean orbital resonance locks, *Nature* **279**, 767–770, 1979.

Yoder, C. F. and S. J. Peale, The tides of Io, *Icarus* **47**, 1–35, 1981.

Yoder, C. F. and W. L. Sjogren, Tides on Europa, in *Europa Ocean Conference*, San Juan Capistrano, 1996.

Yoder, C. F. and E. M. Standish, Martian precession and rotation from Viking lander range data, *J. Geophys. Res.* **102**, 4065–4080, 1997.

Yoshino, T., M. J. Walter, and T. Katsura, Core formation in planetesimals triggered by permeable flow, *Nature* **422**, 154–157, 2003.

Zahnle, K., P. Schenk, H. Levison, and L. Dones, Cratering rates in the outer solar system, *Icarus* **163**, 263–289, 2003.

Zimmer, C., K. K. Khurana, and M. G. Kivelson, Subsurface oceans on Europa and Callisto: Constraints from *Galileo* magnetometer observations, *Icarus* **147**, 329–347, 2000.

Zolotov, M. Y. and E. L. Shock, Composition and stability of salts on the surface of Europa and their oceanic origin, *J. Geophys. Res.* **106**, 32 815–32 828, 2001.